UNIVERSIDADE D
COIMBRA

Renato Ferreira Gonçalves

STUDY OF PVDF SENSOR FOR THE MEASUREMENT OF PRESSURE WAVE ATTENUATION

VOLUME 1

Dissertação no âmbito do Mestrado Integrado em Engenharia Mecânica, Ramo de Energia e Ambiente coorientada pelo Professor José Manuel Baranda Moreira da Silva Ribeiro e pelo Professor Michel Arrigoni e apresentada ao Departamento de Engenharia Mecânica da Faculdade de Ciências e Tecnologias da Universidade de Coimbra.

Junho de 2022

1 2 9 0 FACULDADE DE CIÊNCIAS E TECNOLOGIA UNIVERSIDADE D COIMBRA

Study of PVDF Sensor for the Measurement of Pressure Wave Attenuation

Submitted in Partial Fulfilment of the Requirements for the Degree of Master in Mechanical Engineering in the speciality of Energy and Environment

Estudo do Sensor PVDF para a Medição da Atenuação de Ondas de Pressão

Author

Renato Ferreira Gonçalves

Advisors

José Manuel Baranda Moreira da Silva Ribeiro

Michel Arrigoni

Erwan Tanné

Jury

President	**Professor Doutor Ricardo António Lopes Mendes**
Vowel[s]	**Investigadora Doutorada Joana Filipa Pires D'Oliveira Quaresma**
Advisor	**Professor Doutor José Manuel Baranda Moreira da Silva Ribeiro**

Institutional Collaboration

1 2 9 0 FACULDADE DE CIÊNCIAS E TECNOLOGIA UNIVERSIDADE D COIMBRA

Universidade de Coimbra

ENSTA Bretagne

École Nationale Supérieure de Techniques Avancées Bretagne

Coimbra, Junho, 2022

ACKNOWLEDGEMENTS

This Master's Degree dissertation is definitely a big step in my academic and personal life. It is a step that could only be achieved with the help and support of several parts. Accordingly, I would like to express my most sincere thanks and acknowledgement to everyone who made this project possible.

Firstly, I would like to thank Professor José Manuel Baranda Moreira da Silva Ribeiro, for granting me with this opportunity. I would also like to thank Professor Michelle Arrigoni for welcoming me in ENSTA Bretagne, inserting me in this project and providing me with the necessary resources for the completion of this work.

A special thanks to Post Doctorate Erwan Tanné, who followed my work every step of the way, and always shown himself available to help me overcome any difficulties that appeared during the course of this internship.

I would like to thank Researcher Julien Le Clanche for always being available and supportive during this project.

Lastly, I would like to thank Ines Carmo for all the unconditional support during my internship and for always pushing me to go further.

Abstract

The main purpose of the presented work is the study and calibration of PVDF (Polyvinylidene fluoride) based sensors for dynamic pressure and shock wave measurement.

This sensor is a promising easy to use solution that has a large measurement range and can be stuck or glued to most surfaces, having no need for drilling as opposed to the common piezoelectric sensors (often used for dynamic pressure and shock wave measurement) available in the market.

However, PVDF sensors have some limitations and require some skills to be properly implemented in an acquisition chain. Moreover, the sensors measurements are still very experiment dependant (Arrigoni *et al*. 2018).

Sets of experiments were conducted to study the effects of the sensor's casing on the acquired signal. One set focussed on the adhesive used for gluing the PVDF sensor on the setup while the other focussed on the sensor's shielding and backing. Two different modes of signal acquisition are considered: Voltage mode measurement and Charge mode measurement.

A second set of experiments was conducted to study the capability of PVDF sensors for underwater pressure measurement. A setup was designed to create shock induced cavitation, by shooting a focussed laser pulse to a submerged target.

Interesting results were obtained when measuring dynamic pressure and shock waves generated by cavitation bubble with PVDF sensors. A sensor casing which highly improved the quality of the signal was discovered, which allowed the capture of more accurate and reproducible results.

Keywords: PVDF sensor, Piezoelectricity, Shock induced cavitation, Pressure wave, Cavitation armour, Polyvinylidene fluoride.

Resumo

O principal objetivo da presente dissertação foi o estudo e calibração de sensores baseados em PVDF (Fluoreto de polivinilideno) para a medição de pressão dinâmica e de ondas de choque.

Este sensor é uma solução promissora e fácil de usar que possui uma grande banda de medição e que pode ser fixado ou colado à maioria das superfícies, eliminando a necessidade de furagem das superfícies ao contrário dos sensores piezoelétricos comuns (normalmente usados na medição de pressão dinâmica e de ondas de choque) disponíveis no mercado.

No entanto, os sensores PVDF tem algumas limitações e requerem alguma habilidade para que sejam propriamente integrados numa cadeia de aquisição. Além disso, as medições deste sensor ainda são bastante dependentes da experiência (Arrigoni *et al*. 2018).

Várias experiências foram realizadas de modo a estudar os efeitos do invólucro do sensor no sinal obtido. Parte das experiências focou se no tipo de adesivo utilizado para a fixação do sensor na instalação, enquanto a outra parte focou se na proteção e apoio do sensor. Dois diferentes modos de aquisição de sinal foram considerados: medição em modo de voltagem e medição em modo de carga.

Um segundo conjunto de experiências foi realizado para estudar a capacidade de medição de pressão dos sensores PVDF quando submersos. A criação de um *setup* experimental permitiu a geração de cavitação induzida por choque através do disparo de um pulso laser para um alvo submerso.

Resultados interessantes foram obtidos ao utilizar sensores PVDF para a medição da pressão dinâmica e ondas de choque geradas por bolhas de cavitação. Um invólucro para o sensor PVDF que permite a obtenção de resultados com maior precisão e reprodutibilidade foi descoberto.

Palavras-chave: Sensor PVDF, Piezoeletricidade, Cavitação induzida por choque, Onda de Pressão, Armadura de cavitação, Fluoreto de polivinilideno.

Contents

LIST OF FIGURES

LIST OF TABLES

LIST OF SYMBOLS AND ACRONYMS/ ABBREVIATIONS

List of Symbols

A [mm^2] – Surface area of a PVDF film

C [pF] – Capacitance of the acquisition chain

C_w [m/s] – Speed of sound in water

d_{31} [pC/N] – Piezoelectric coefficient of a PVDF film along the film's thickness direction

d_{32} [pC/N] – Piezoelectric coefficient of a PVDF film along the machine stretching direction

d_{33} [pC/N] – Piezoelectric coefficient of a PVDF film along the transverse stretching direction

F [N] – Applied force

h [mm] – Distance between PVDF sensors

K_{PVDF_2bar} – PVDF calibration coefficient for 2 bar

K_{PVDF_4bar} – PVDF calibration coefficient for 4 bar

K_{PVDF_6bar} – PVDF calibration coefficient for 6 bar

K_{PVDF_8bar} – PVDF calibration coefficient for 8 bar

K_{PVDF_8642} – PVDF global calibration coefficient

P [Pa] – Applied pressure

P_{PVDF} [Pa] – Pressure measured by PVDF sensor

P_{Target} [Pa] – Expected target pressure

Q [pC] – Charges generated by the sensor

R [Ω] – Input resistance of the acquisition chain

s [mm^2] – Cross section area of a PVDF film

S [mm^2] – Active area of a PVDF sensor

t [mm] – Thickness of a PVDF film

t [s] – Time

U [V] – Voltage generated by the sensor

λ – Laser pulse wavelength

τ [ms] – Timelapse of the primary shock measurement between two PVDF sensors

Acronyms/Abbreviations

ENSTA Bretagne – Ecole Nationale Supérieure de Techniques Avancées Bretagne

FCTUC – Faculdade de Ciências e Tecnologia da Universidade de Coimbra

ISL – Institut Saint-Louis

PVDF – Polyvinylidene fluoride

PMMA – Poly (methyl methacrylate)

1. INTRODUCTION

ProBalCav, a play on the words Protection, Balistique and Cavitation, is a project that is studying the possibility of creating a ballistic armour based on shock induced cavitation. It is thought that by inducing cavitation the energy delivered to the armour upon impact will be transferred to a bubble which will then disperse and dissipate the majority of the energy of the shock wave and therefore decrease the amount of damage that the wave could potentially cause.

A traditional approach to shock wave measurement is the use of piezoelectric sensors which are generally bulky and require flush mount on a pencil or perch, for the measurement of the pressure profile of the shock wave. For this reason, the use of these sensors is not always suited for all applications since some models and experimental setups have such a reduced scale that the integration of these sensors is simply not possible. Additionally, most piezo electric sensors can only measure a small range of pressures and have an acquisition speed of about 300 kHz which further limits their use.

To overcome this, an easy-to-use solution, based on PVDF piezoelectric polymers, is being considered. PVDF sensors possess an active area which be as small as $1mm^2$, and it can be stuck or glued in most surfaces with no need for drilling. Furthermore, PVDF sensors have a measurement range of a few kPa to several GPa.

However, PVDF shock gauges are still very dependent on the experimental setup and are not fully understood, therefore this work will focus on the study and understanding of PVDF pressure gauges behaviour, as well as the in obtaining the calibration of this sensor for larger scale experiments as well as for future application in the ProBalCav project

1.1. Objectives and Motivation for this Study

The main purpose of the presented work is the study and calibration of PVDF (Polyvinylidene fluoride) based sensors for pressure and shock wave measurement trough experimentation, for future use in the ProBalCav project.

With a large measurement range and small size which allows for their use in most scenarios, PVDF sensors can be considered a low-cost solution for shock and blast wave measurements. However, a better understanding of these sensors is required for proper integration of PVDF sensors to be achieved, not only on ProBalCav but on other future projects as well.

PVDF sensors are a non-intrusive solution which can be used to monitor future shield armour or any other shock wave analysis experiment.

1.2. Adopted Methodology

In this document 5 chapters can be found in a logical and sequential order, which also reflects the progress of the work that was conducted, these chapters are the following:

The first chapter is destined to the introduction of the theme and the explanation of the relevance of the objectives for the study as well as the methodology used to do so.

In second chapter all the relevant literature for this study is presented.

The third chapter presents the findings and the results of the experiments conducted in the calibration experimental setup, and the steps taken to ensure the obtained results were as trustworthy as possible.

The fourth chapter shows the data obtained from the use of PVDF sensors in a more complex experimental setup, in which a shock induced cavitation bubble was created with the use of a laser pulse.

In the last chapter the conclusions derived from the conducted experiments are presented as well as perspectives and possibilities for future tests that will allow for a deeper experimentation and understanding of PVDF sensors and their use in shock wave measurement.

2. FRAMEWORK

ProBalCav is a project that was born due to the cooperation of 3 entities, ESNTA Bretagne, IJLRDA (Institut Jean Le Ronde d'Alembert) and Olea Technology.

The main goal of this project is the study and development of a ballistic protection based on cavitation. Through the work of Grandjean *et al*., 2012 on shock-bubble interaction and the work of Fourest *et al*., 2014 on hydrodynamic ram, it was realized that there could be some benefits in transferring the energy of an impact into a bubble, since the bubble dynamics, that is, its expansion and contraction, are energy consuming. Furthermore, there is a beneficial bubble effect that disperses the energy of the impact in multiple directions, instead of keeping a large energy concentration in one single direction.

2.1. Background of PVDF Sensors

As mentioned before, the shock measurement sensors in the market have a great number of limitations regarding versatility, use flexibility, mounting and range of measurement. For this reason, in this study a simpler solution (PVDF shock gauges) that can be used for a higher range of pressure and be easily applied to any surface via a bonding agent will be studied.

2.1.1. Piezo- and Pyroelectricity

Ever since piezoelectricity was discovered by Jacques and Pierre Curie in 1880, in some simple asymmetrical crystals, this phenomenon has kept minds excited. If a mechanical stress is applied to a piezo material, electrical charges will be generated. On the other hand, when an electrical field is applied to this same type of material a mechanical strain will appear. These two effects are denominated the direct and reverse piezoelectric effects, respectively. Also, in materials that show pyroelectric properties, electrical charges will be generated under the effect of a temperature gradient. A poled ferroelectric material is a material that exhibits both piezoelectric and pyroelectric properties.

In 1969 Kawai found that the semi-crystalline PVDF (polyvinylidene fluoride) polymer gains strong ferroelectric properties after being subjected to the effects of both mechanical stretching and the application of an electrical field (Ueberschlag 2001).

2.1.2. PVDF Sensor

Poled PVDF films with a high level of polarization reproducibility, are achieved through the cycling poling process that was developed by Dr Bauer from the Institut de Saint-Louis (ISL), France. This process begins with a low electrical field, at this stage the unpoled PVDF film is cycled through a series of loops, until a consistent behaviour is present. After this stage, higher electrical fields are applied in order to achieve the desired level of polarization.

After the PVDF piezoelectric film is produced electrodes must be added so that electrical signals can be acquired. One electrode is deposited in each side of the film and in such a way that they "cross" each other forming an area that has an electrode on each side as shown in Figure 2.1. The area of film that is covered by an electrode on both sides is called the active area and is the only part of the film that will produce an electrical signal.

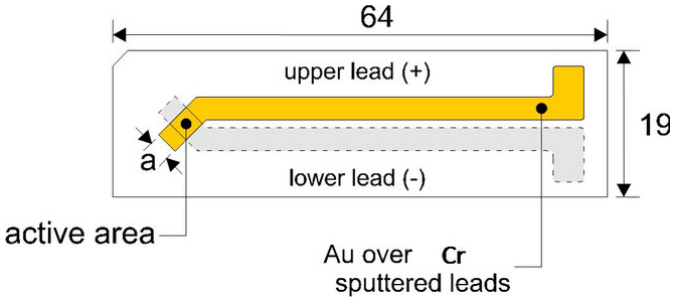

Figure 2.1. Physical specification of a 25-µm thick Bauer shock gauge **("Products - Aifp-Bauer", accessed on the 31st of May of 2022, in: https://aifp-bauer.fr/)**.

PVDF sensors manufacturing can have different variations, regarding the type of mechanical stretching, i.e., uni-axially stretched film in which case the PVDF film is only stretched in the machine direction, or bi-axially stretched film when the film is stretched in both the machine and transverse directions, the latter method confers better overall properties (a more uniform thickness, better isotropic properties, no wrinkling when heated and a better long-term stability). The other major variant in PVDF shock gauges manufacturing are the electrodes that are deposited in the film, these can vary in material and width (when the width is altered so is the size of the active area). There are a few options for the metal used in the electrodes, since many different highly conductive metals can be used, among the most commonly used for PVDF gauges are aluminium, copper, gold and platinum (usually covered with gold). The size of the active area can be as small as 1 mm^2 (1 mm x1 mm) and

go up to 25 mm^2 (5 mm x 5 mm). While smaller sensors are more versatile and can be used for smaller scales, they generate less charges when compared to sensors with larger sensitive areas.

Figure 2.2. Photograph of a 25-μm thick Bauer shock gauge.

The PVDF gauges used in this work have been manufactured by AIFP, from a highly reproducible PVDF film using the patented process of the ISL (Institut Saint-Louis), Figure 2.2 shows one of the sensors in question. With a sensitive area of 9 mm^2 (3 mm x 3 mm), and electrodes of gold over platinum on a 25 μm by-axially stretched PVDF film, the properties of these PVDF Bauer shock gauges are as presented in Table 2.1.

Table 2.1. PVDF properties corresponding to the used batch of sensors (information provided by AIFP)

Property	Value	Unit
Thickness (t)	24 ± 1	[μm]
Active area (S)	9	[mm^2]
Polarization	9 ± 3	[$\mu C/cm^2$]
Piezoelectric coefficient along the thickness axis ($\mathbf{d_{33}}$)	23 ± 0.4	[pC/N]

PVDF films possess three piezoelectric coefficients, one for each axis, these are d_{31}, d_{32} and d_{33}, these coefficients correspond to the machine direction stretching axis (axis 1), the transverse direction stretching axis (axis 2) and the polarization direction axis or thickness axis (axis 3), respectively, a representation of the axes is show in Figure 2.3.

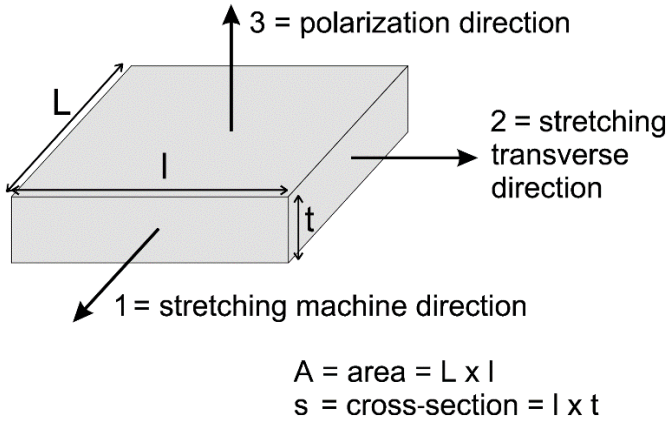

Figure 2.3. Axis definition of piezo elements (Ueberschlag 2001).

According to Ueberschlag 2001, when the film is used in thickness mode, i.e., the force is applied to the films surface, only the piezoelectric coefficient of the third axis, d_{33}, is to be considered and the charge, Q, generated by the applied force, F, is:

$$Q = d_{33} \cdot F \tag{2.1}$$

However for shock wave measurement, it is more relevant to obtain the pressure rather than the force, therefore equation (2.1) can be modified, considering the relations (2.2) and (2.3):

$$P = \frac{F}{S} \tag{2.2}$$

$$Q = C \cdot U \tag{2.3}$$

If only (2.2) is considered the resulting equation, (2.4), gives the measured pressure P, as the quotient of the charges created by the sensor, Q, and the piezoelectric coefficient , d_{33}, multiplied by the active area of the sensor, S.

$$P = \frac{Q}{d_{33} \cdot S} \tag{2.4}$$

However if both relations, (2.2) and (2.3), are considered, the result is equation (2.5), in which the pressure, P, measured by the sensor is given by the quotient of the capacitance of the acquisition chain, C, multiplied by the voltage that is generated by the sensor, U, and the piezoelectric coefficient , d_{33}, multiplied by the active area of the sensor, S.

$$P = \frac{C \cdot U}{d_{33} \cdot S} \tag{2.5}$$

2.1.3. Acquisition Chain

As presented in the previous section, through equations (2.4) and (2.5), pressure can be obtained either from reading the charge generated between the poles of the PVDF sensor or by reading the voltage emitted by the sensor.

Obtaining these different signals requires different types of equipment and consequently different acquisition chains.

2.1.3.1. Voltage Mode Measurement

Measuring the voltage generated by the PVDF film is the simplest way to measure the electrical signal that is delivered by the Piezo film. This can be easily achieved with a simple acquisition chain, in which, for example, the sensor is directly connected to an oscilloscope, as presented in Figure 2.4. Voltage mode acquisition chain schematic.Figure 2.4.

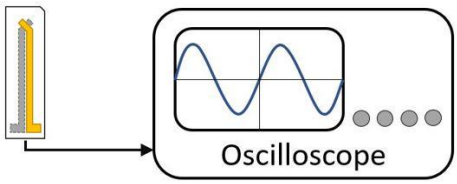

Figure 2.4. Voltage mode acquisition chain schematic.

According to Ueberschlag, 2001 if the required measurement is the force versus time representation, the condition $RC >> t$, where R is the input impedance and C the acquisition chain's capacitance, is necessary. If compliance with this condition fails, the captured signal will be a time derived representation of the force applied to the sensor.

2.1.3.2. Charge Mode Measurement

Rather than the voltage, the charges generated by the poles of the sensor can also be acquired. This can be accomplished via a regular charge amplifier, provided that enough bandwidth is available, an acquisition chain example for this option is presented in Figure 2.5.

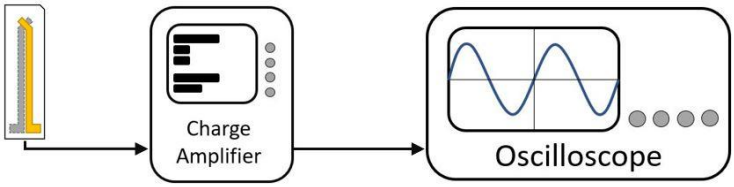

Figure 2.5. Charge mode acquisition chain schematic.

2.2. Examples of PVDF Gauge Measurements

In the literature PVDF sensors have been used in various experiments for blast and pressure wave measurements. In this chapter two examples in which PVDF has been used are presented. In each case a different measurement mode was used.

2.2.1. Shock Tube Experiment by M. Arrigoni

In Ecole Nationale Supérieure de Techniques Avancées Bretagne (ENSTA Bretagne), some experiments in which PVDF sensors were used have been conducted, one of these studies was made by M. Arrigoni using a Shock tube that is present at ENSTA Bretagne, Figure 2.6, an article about this study was written and published, (Arrigoni *et al*. 2018). This subchapter will focus on the experiments performed and the obtained results.

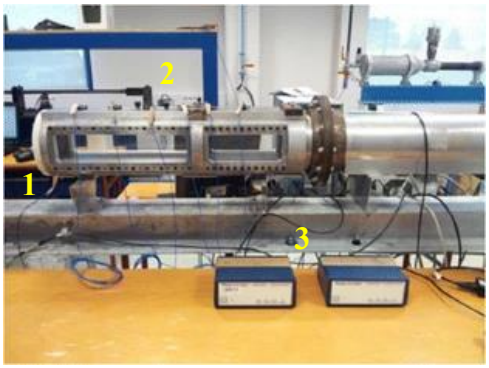

Figure 2.6. End of the shock tube showing windows (1) , sensors positions (2), and conditioners (3), (Arrigoni et al. 2018).

According to Arrigoni *et al*. 2018, PVDF gauges are quite difficult to integrate in an acquisition chain and the results are strongly "experiment dependent". In this experiment the sensor was electrically shielded. The gauge was connected to a charge amplifier through a 5-m long coaxial wire, which then was connected to a deported oscilloscope. The output electrical charge of the PVDF gauge was correlated with the pressure which was measured by calibrated PCB® sensors.

Before starting the experiments an analytical solution of the expected overpressure, that would be reached at the end of the shock tube was calculated using the ("WiSTL Gas Dynamics Calculator" 2008). The shock tube at ENSTA Bretagne has a 92 cm long driver section and 3.72 m driven section, its cross section is an 8 × 8cm square. The driver and driven sections are separated by a Mylar® film that will burst when the hydrostatic pressure inside the driver section is higher than 6.2± 0.1 bar (absolute). After the calculations were completed a value of around 4.96 bar (absolute) for the reflected pressure was calculated, and therefore was expected to be measured for the experiments that followed.

Four different sensors were then mounted on the end of the shock tube, two PVDF Bauer shock gauges, denominated by PVDF_Y and PVDF_J2, and two PCB® which were distinguished by their serial numbers, PCB no. 28292 and PCB no. 28293.

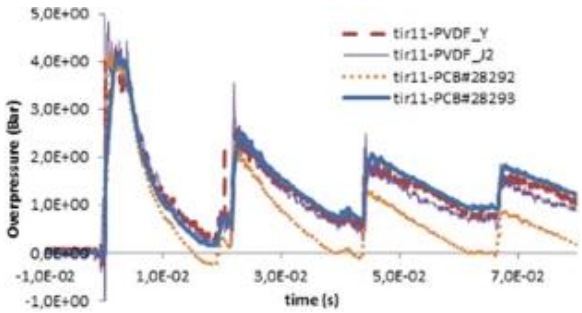

Figure 2.7. Example of time-resolved signals given by PVDF and PCB® sensors for shot no. 11, (Arrigoni et al. 2018).

Upon each shot, the measured pressure signals were compared to each other. Figure 2.7 represents an example of the obtained results by considering calibration coefficients given by the manufacturer for PCB® sensors, for PVDF sensors a fitting calibration coefficient was used so that they match data recorded by the calibrated PCB® sensors.

The authors wrote that, by observing and comparing the signals of the four sensors, for each shot, the results suggest that the different sensors show the same rising front, this is shown in Figure 2.7, and that if indeed some differences are present in these signals these cannot be observed due to the limited bandwidth of the Kistler charge amplifier (max 150 kHz) that was used.

In this experiment the sensors detect the arrival of the shock front at the end of the shock tube which corresponds to the overpressure calculated analytically. The measured overpressure of the reflected shock is around 4 bar (relative), this corresponds to approximately 5 bar (absolute), which is the value that was analytically foresaw. Each peak that is observed corresponds to the waves going back and forth in the tube.

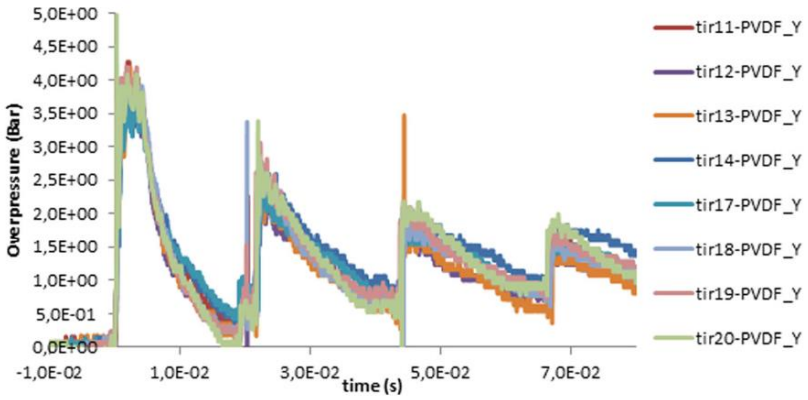

Figure 2.8. Pressure signals measured by the PVDF_Y sensor at the end of the shock tube, (Arrigoni et al. 2018).

The results show that PVDF signals are noisier than PCB ones, it was concluded by the authors that this happened because the vertical scale of the oscilloscope was 200 mV/division in 8 bits, which is not an optimal setting for the acquisition of the signal when considering the PVDF signal amplitude.

The recorded PVDF_Y sensor signals for each shot, show a rather good reproducibility, as shown in Figure 2.8. However, PVDF sensor reproducibility is not quite as good as the reproducibility observed when using PCB® sensors, as illustrated in Figure 2.9.

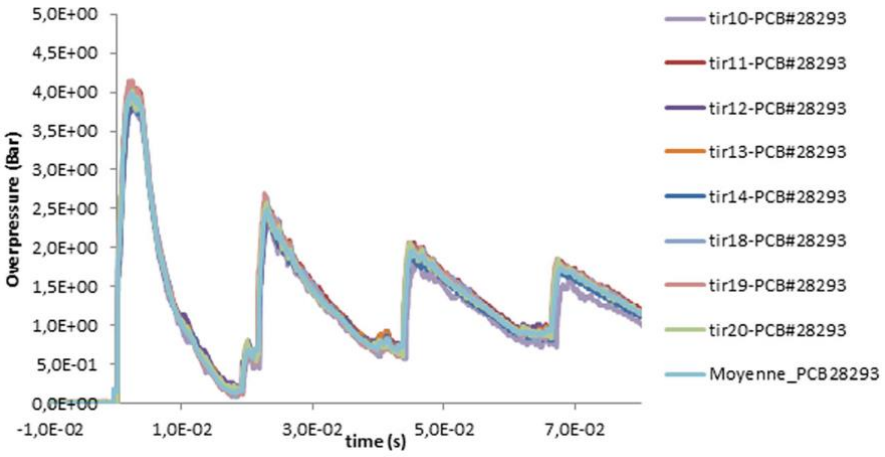

Figure 2.9. Pressure signals measured by the PCB SN no.28293 at the end of the shock tube, (Arrigoni et al. 2018).

The authors conclude that proposed blast sensor based on a poled PVDF film shows interesting responses for blast loading measurements. Additionally, this sensor is easy to mount on the target with no need for drilling.

2.2.2. Study of underwater pressure wave induced by bubble implosion

Han *et al*. in 2021, designed an experiment to measure the underwater pressure wave generated by the implosion of an underwater laser generated cavitation bubble.

The experimental setup, as represented in Figure 2.10, consisted of a pulsed laser that would fire a laser pulse, with a 5 ns duration and a $\lambda = 532$ nm wavelength, into a 6×6 cm cubic container filled with demineralized water, in order to generate a size-controlled bubble. To measure the pressure of the bubble's collapse, a PVDF shock gauge connected in voltage mode to an oscilloscope was used. This sensor had to be accurately aligned with the centre of the bubble to get a viable measurement of the underwater pressure variations that are associated with the bubble dynamics.

Furthermore, it was necessary to observe the bubbles behaviour at a high rate. This was achieved via a high-speed camera recording at 120 000 fps, with a resolution of 128 x 256 pixels. To shield the camera from the laser's lighting an interferential filter for the same wavelength of the laser's pulse was used. The backlight illumination was obtained by using a continuous light-emitting diode (3 W LED) directly facing the high-speed camera as shown in Figure 2.10.

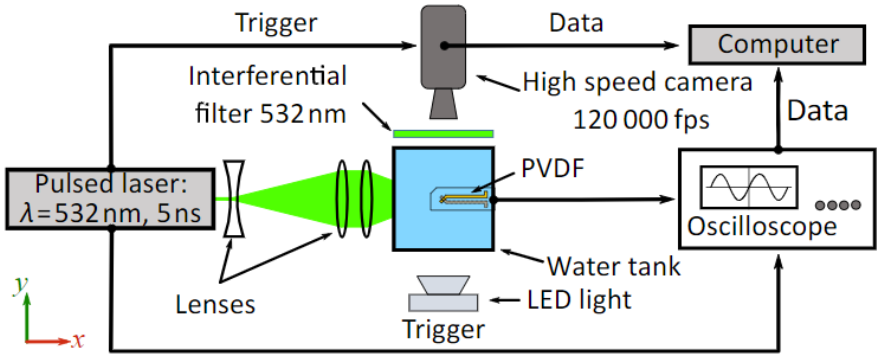

Figure 2.10. Schematics of the experimental set-up,(Han et al. 2021).

The pressure's acquisition chain is composed of a PVDF sensor, an oscilloscope and a computer as shown in Figure 2.10. The position of the PVDF sensor relative to the bubble is presented in Figure 2.11. If the sensor is off axis regarding the bubble centre, the curvature of the shock front will not remain frontal to the active area of the sensor, for this reason it is necessary to ensure that the bubble centre is aligned with the PVDF sensor's centre along the z axis as illustrated in Figure 2.11.

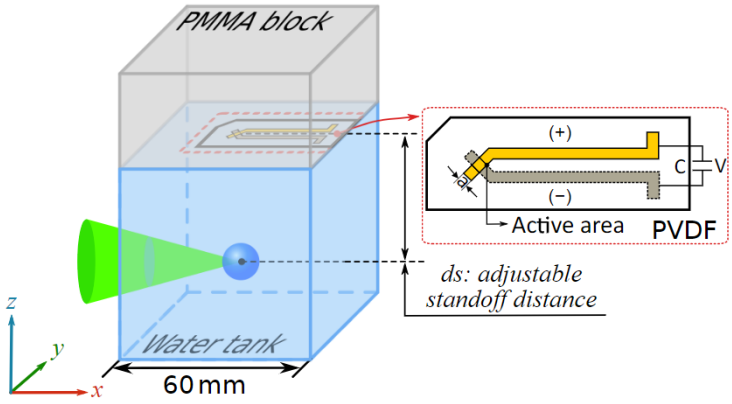

Figure 2.11. Schematic of the relative position of bubble in the water tank, the installation position of the PVDF sensor and the structure of the PVDF sensor,(Han et al. 2021).

The backing of the sensor was assured by a 40 mm thick block of poly (methyl methacrylate) (PMMA) since this material's impedance is similar to that of PVDF. After the sensor is stuck to the block, the block is placed directly on top of the tank, water is added in

such a manner that no air is present inside the container, ensuring that air has no interference in the measured signal.

The study of the evolution of a focused laser generated bubble that was created at different distances, according to the z axis, represented in Figure 2.11, was possible through the two image sequences presented in Figure 2.12. As previously mentioned, these images were taken at 120 000 fps with a frame size of 128 x 256 pixels.

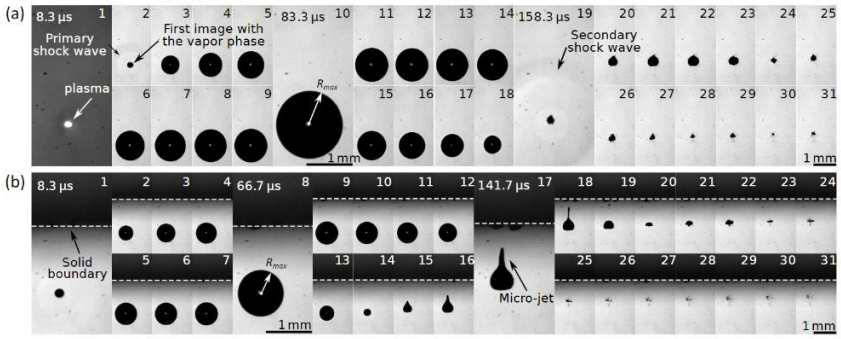

Figure 2.12. (a) Dynamics of a cavitation bubble far from a solid boundary. (b) Dynamics of a cavitation bubble in the close presence of a solid boundary. The time between each image is constant, and the frame rate is 120 000 fps,(Han et al. 2021).

According to the authors of this study, when the bubbles collapse away form a solid boundary, in which case a lower amount of hydrostatic pressure gradients have influence on the bubble's dynamics the bubble collapses in a quasi-spherical manner, this phenomenon can be observed in Figure 2.12(a). To achieve a perfectly spherical collapse no hydrostatic pressure gradients can influence the bubble. However, if a solid boundary that is close to the bubble is present, the bubble will collapse in an asymmetrical manner which has the potential to generate a high-speed liquid micro-jet. This jet is directed toward the solid boundary.

Pressure waves are emitted into the water due to the fast expansion and contraction of the bubble. The active area of the sensor is lightly deformed when it is compressed by these pressure waves, and due to the piezoelectric nature of poled PVDF, a voltage potential is generated between the poles of the PVDF sensor.

Since the sensor was connected directly to the oscilloscope, i.e., in voltage mode, and the obtained signal was a potential difference, the relation used by the authors, to correlate pressure with voltage is given by equation (2.5).

To obtain a pressure value form the voltage signal, U, using the previous equation a few parameters need to be known. Among them the piezoelectric coefficient, d_{33}, and the sensors active surface, S, are both provided by the sensor's supplier. Consequently, only the acquisition chain's capacitance needs to be measured in order to obtain the pressure reading.

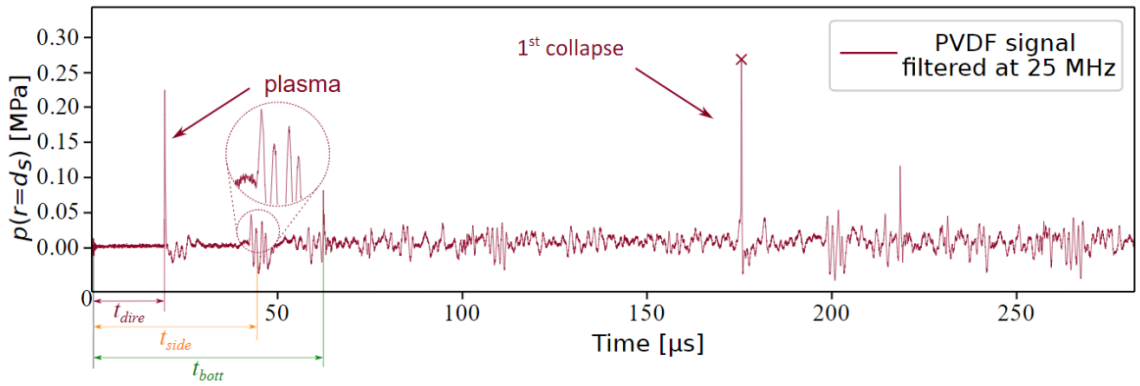

Figure 2.13. Quantitative measurement by a PVDF sensor,(Han et al. 2021).

Identifying the different peaks of the signal, and the wave reflections that caused them is possible, since the position of the bubble centre as well as the tank's dimensions and the moment in time in which the plasma is generated are all known parameters. Knowing these, it is possible to calculate the arrival time of the generated waves, this identification is represented in Figure 2.13.

To further study the accuracy of the measurements obtained by using a PVDF gauge, an analytical solution of the wave propagation was calculated using the Gilmore model. The pressure obtained by this analytical wave propagation model and the experimentally obtained pressure through PVDF sensor measurement are compared in Figure 2.14 (b). The peak generated by the first collapse of the bubble is enlarged and represented in Figure 2.14 (c). This image shows that the curve obtained by the analytical model and the curve obtained by direct pressure measurement using PVDF are not similar, however the maximum pressure value, i.e., the peak of the experimental curve is matched by the peak of the curve predicted by the Gilmore model with a relative difference of 17%.

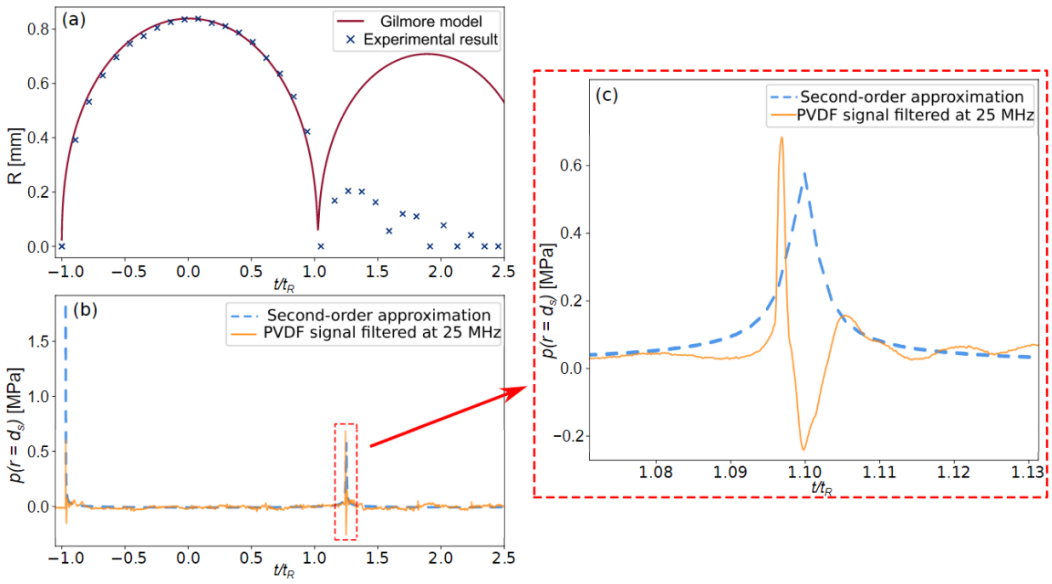

Figure 2.14. (a) Bubble radius evolution: comparison between experimental data and Gilmore model. (b) Comparison of PVDF sensor and wave propagation model pressure. (c) Zoom of the peak pressure caused by the bubble collapse.,(Han et al. 2021).

This study presented bubble collapse experiments for different distances from a solid boundary. The bubble dynamics were recorded with a high-speed camera and the pressure was quantitatively measured using a PVDF gauge, the obtained data was correlated with the Gilmore analytical model.

According to the authors PVDF presents a good capability to quantitatively measure underwater pressure waves.

3. PVDF STUDY AND CALIBRATION

The previous examples, shown in subchapter 2.2 - Examples of PVDF Gauge Measurements, are good examples of the capability of PVDF gauges to give a quantitative measurement of pressure. However, PVDF sensors still require some effort to be integrated in a proper acquisition chain, furthermore, the obtained results are very dependent on the experimental setup in which they are integrated, (Arrigoni *et al*. 2018).

For this reason, it was proposed, at ENSTA Bretagne, that a study should be conducted, to better understand the working of PVDF sensors before integration this sensor on lager experiments linked to the ProBalCav project. This study should focus on the impact of the sensor's direct surroundings, more specifically the impact of the sensor's casing and backing, on the measurements of this sensor.

3.1. PVDF Limitations

Being composed of a thin PVDF film, only 25µm thick, this sensor presented some challenges to be integrated without being damaged. Three major limitations emerged when operating with PVDF: Connection, Fixation and Shielding.

3.1.1. Connection

To integrate this sensor in an acquisition chain, it obviously needs to be electrically connected. Despite seeming an easy task, discovering a way to connect the sensor without damaging the gold over platinum deposition that composes the sensors electrodes, was arduous at the least.

Such a connection was possible using a DEXTER® small spring clamp, to which wires were glued to its extremities and later covered with copper to achieve a smooth finish, effectively converting a regular clamp into a connector suitable for use with PVDF sensors. Figure 3.1 (a) and (b), show the previously referred connector as well as the modifications that were added to the clamp to achieve said connector.

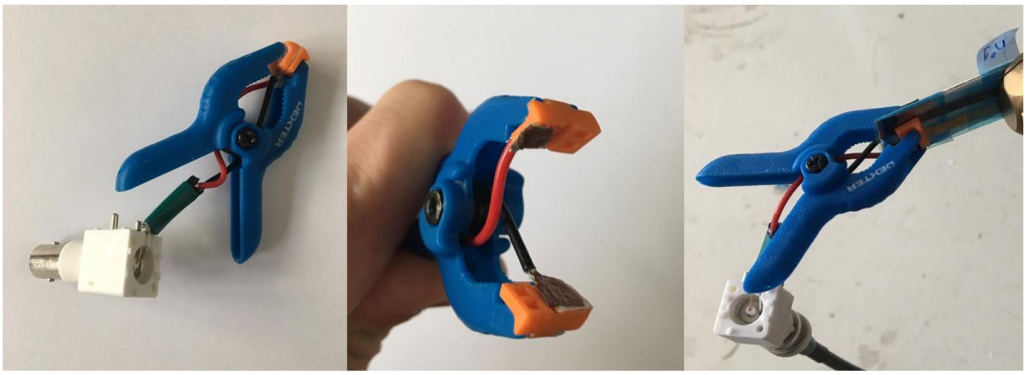

(a) (b) (c)

Figure 3.1. (a) Clamp based connector; (b) View of the electrodes added to the clamp; (c) Example of a PVDF connected to a 3-meter-long BNC coaxial cable through clamp-based connector.

This connector allowed for an easy manner to connect and disconnect the PVDF sensor to the acquisition chain, while minimising the damage caused by scratching on the film's electrodes.

3.1.2. Fixation

As previously mentioned, this sensor does not require drilling or any type of machinery to be applied to an experimental setup, instead, this sensor can be glued or stuck to a surface with the aid of a bonding agent.

The selection of the bonding agent, however, should not be made thoughtlessly since it is a rather important part of the sensor's casing. If chosen incorrectly the adhesive can damage the sensor (upon removal of the sensor) and/or greatly influence its measurements. According to Ueberschlag, 2001, both epoxy and cyanoacrylate glues are suitable candidates for bonding agents, provided that a thin layer of adhesive is used. If prototyping is the purpose, double sided tape can also be an option since these are generally easy to use.

Additionally, two other bonding agents were proposed, repositionable glue and silicone grease, since they propose the possibility to fix the sensor to the target with the premise that after use the sensor can be easily removed and cleaned with no significant damage to the film or electrodes.

Preliminary tests revealed that repositionable glue was not a suitable candidate for this, removing parts of the gold deposition when removed and consequently defeating the purpose for its use. Double sided tape poses the same problem and was discarded for the same reason.

Due to material availability and the already mentioned problems with some of the adhesives, the choices were reduced to two options: cyanoacrylate glues and silicone grease. To further study the effects of each bonding agent on the sensor's signal a few experiments were conducted and are presented 3.3.1 Bonding Agent Experimental Results.

3.1.3. Shielding

Since PVDF sensors are very sensitive to their surroundings, two types of shielding for this sensor must be considered: mechanical shielding, to confer a higher mechanical resistance to the sensor, and electromagnetic shielding, to shield the sensor from possible parasite signals that could be captured by the sensor.

Electromagnetic shielding was accomplished by adding a layer of aluminium tape around the sensor's casing and connecting it to the electrical ground, effectively creating a Faraday cage shielding the sensor from exterior signals.

For the mechanical shielding, a thin layer of vinyl tape was added to the sensor, the purpose of this vinyl shielding was to protect the sensor from being damaged by manipulation or even by the bonding agent itself.

To study the effects of adding shielding to the sensor, experiments were conducted, and their results are presented in section 3.3.2 Tape Shielding Experimental Results. The vinyl tape shielding was added in three distinct ways:

1. Double-sided Shielding – the PVDF sensor is inlaid with vinyl tape shielding on both sides (The tape shielding provides a higher mechanical resistance to the sensor), glued with cyanoacrylate glue to a metal cap, Figure 3.5, that connects to the experimental setup, Figure 3.6. An illustrative representation of this type of shielding can be observed in Figure 3.2.

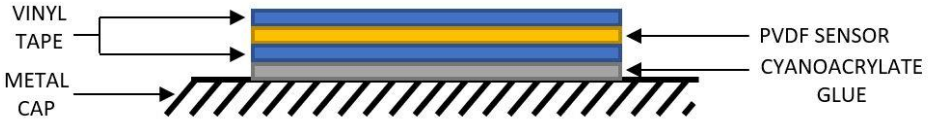

Figure 3.2. Illustrative example of PVDF sensor with double-sided shielding.

2 One-sided shielding – the PVDF sensor is inlaid with tape shielding only on the back side and is glued with cyanoacrylate glue to the previously mentioned metal cap, which acts as the sensor's casing. A representation of one-sided shielding is presented in Figure 3.3.

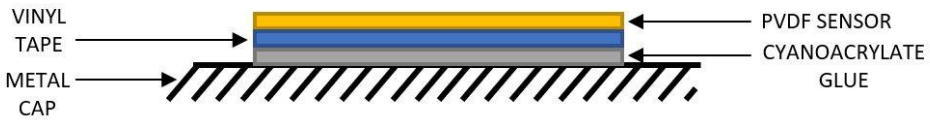

Figure 3.3. Illustrative example of PVDF sensor with one-sided shielding.

3 No shielding – the PVDF sensor has no added layers of vinyl tape, thus it is directly glued with cyanoacrylate glue, Figure 3.4, to the sensor holder which connects it to the experimental setup.

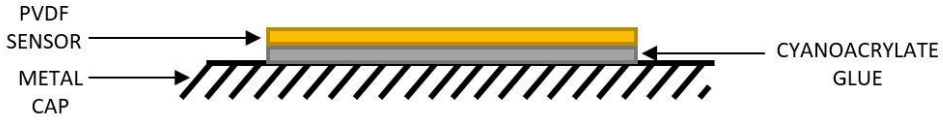

Figure 3.4. Illustrative example of PVDF sensor without shielding.

The sensor holders, used to attach the sensors to the experimental setup, presented in the following section, 3.2 Experimental Setup, were composed of a metal cap, to which the sensor, with or without shielding, was glued with a cyanoacrylate adhesive. These holders can be observed in Figure 3.5 (a) and Figure 3.5 (b).

(a) (b)

Figure 3.5. (a)Open sensor holder; (b) Closed sensor holder

3.2. Experimental Setup

The experimental setup needed to ensure 3 major functions, firstly, fast assembly and disassembly of different sensors to and from the setup was necessary, moreover the possibility to have 1 or 2 sensors measuring the applied pressure at the same time was required and lastly it was essential to control the pressure applied to the sensors.

On that account, in the designed experimental setup, the compressed air from the laboratory's main supply at a pressure of around 7 bar, is treated at an air conditioning and compressing table, where full control over the pressure added to the compressed air bottle is allowed. This table has the potential to reach pressures in the range of 1 to 40 bar, however, due to constraints related to the remaining equipment only 8 bars were reached in these experiments. After the pressure is selected, the air is kept in the bottle. At the trigger time, $t = 0$s, the five-way two-position solenoid valve is activated, and the air is released into a small compartment, at the end of the experimental setup, of negligible volume where the sensors are located.

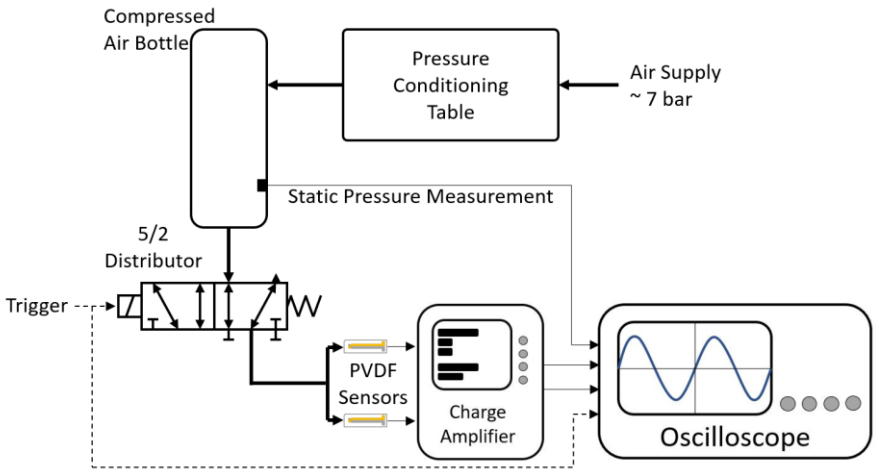

Figure 3.6. Schematic of the setup for charge mode measurement with 2 PVDF sensors.

As previously mentioned, the compartment at the end of the setup can hold 2 sensors at the same time. The sensors used for this experiment were PVDF sensors and PCB sensors for comparison purposes. Additionally, a static pressure sensor in the compressed air bottle was used, so that an accurate measurement of the pressure inside the bottle could be obtained.

Signals acquired from all the sensors are recorded, this includes PVDF sensor, PCB sensors and the static pressure sensor at the compressed air bottle. A schematic of the described setup is presented in Figure 3.6.

Two different ways for measuring with PVDF sensors were considered, these were the already mentioned voltage and charge measurement modes. Consequently, the acquisition chain was altered according to the requirements of each measurement mode.

3.3. Experimental Results

This section presents various results from the performed experiments, which were conducted to attempt to find a suitable set of conditions in which PVDF sensors present the most accurate and reproducible results. The collected data form these experiments was treated in Python using *Jupyter Notebook* from ANACONDA.

3.3.1. Bonding Agent Experimental Results

Experiments were conducted using the 2 different bonding agents mentioned in section 3.3.1, silicone grease and cyanoacrylate glue, for each adhesive several shots were made, with different acquisition modes. Ultimately, all the tests suggested the same result, which is that silicone grease, although a promising candidate for prototyping purposes, shows a higher noise level and less reproducibility that cyanoacrylates. Cyanoacrylate glues on the other hand, show very promising results in terms of high reproducibility and fewer oscillations. Figure 3.7 (a) and (b) show examples of the acquired signals for each of the two bonding agents.

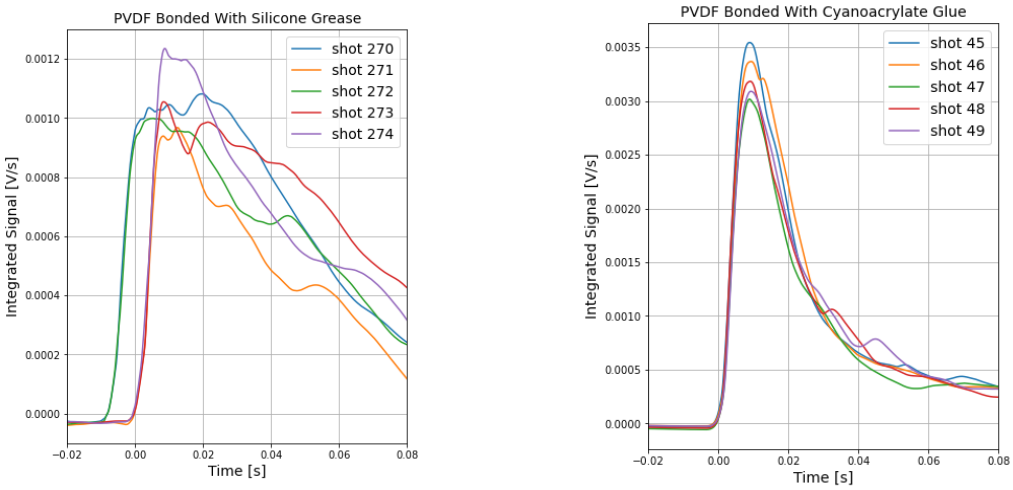

(a) (b)

Figure 3.7. (a) PVDF bonded with silicone grease voltage mode measurement integrated signal acquired with a Tektronix® oscilloscope (model: MSO4034); (b) PVDF bonded with Cyanoacrylate glue integrated voltage mode measurement signal acquired with a portable data recorder (model: 1-GEN3i-2), tests conducted for a pressure of 6 bar.

It is though that the difference in the obtained signals is due to the high discrepancy in bonding strength between the adhesives, i.e., since cyanoacrylates are strong adhesives that harden after drying, the sensor remains in the same position for all the conducted tests. Unfortunately, this is not the case with silicone grease, since silicone grease does not harden it is possible that the sensor shifts position with each of the applied pressure cycles, also it is possible that grease allows for uneven deformation of the active surface adding noise to the measured signal.

3.3.2. Tape Shielding Experimental Results

In order to achieve a better understanding of the impact, of using different layers, on the sensors' signals various tests were conducted. Cyanoacrylate glue was the chosen adhesive seeing that based on previous experiments it would be the option that induced less uncertainty in the results. Given that it was only possible to have two sensors simultaneously connected to the experimental setup the tests were directed in a specific order that allowed for meaningful comparison of the signals. Both the order of experiments and the pairs of sensors simultaneously attached to the end of the setup were as follows:

1. PVDF sensor with **two-sided shielding** and PVDF sensor with **one-sided shielding**.

2. PVDF sensor with **one-sided shielding** with PVDF sensor with **no shielding**.
3. PVDF sensor with **no shielding** alongside **PCB® 113B21 sensor** (serial number (SN) 21794).

The pressures achieved in the experiments were of 2, 4, 6 and 8 bar. The experimental setup remained unaltered, aside from the acquisition chain since measurements were made both in charge and in voltage mode.

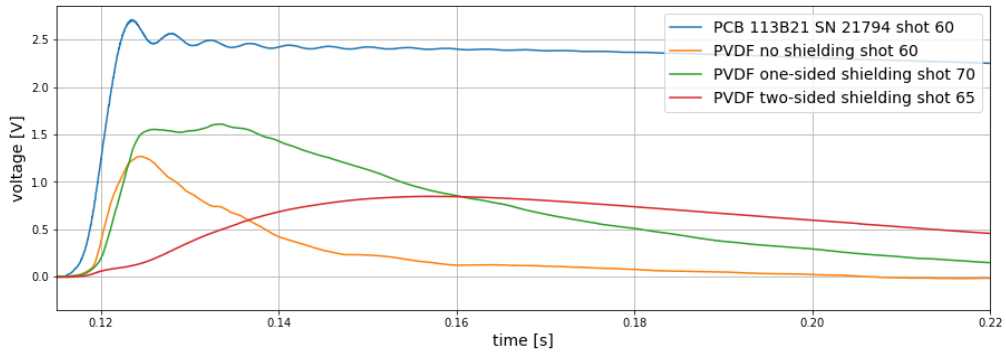

Figure 3.8. PVDF sensors (with different shielding) and PCB® sensor signals for a pressure of approximately 8bar measured in charge mode signal acquired with a portable data recorder (model: 1-GEN3i-2).

Figure 3.8 shows an example of the signals obtained from the different sensors when measured in charge mode. Results indicate that the sensor's casing greatly impacts the signal emitted by the sensor. Among the parameters of the PVDF signal that are affected by the shielding, the rising speed is evidently the most affected. Sensors with different levels of shielding return signals with different rising times, being the one with the highest shielding level, i.e., two-sided shielding, the one that produced the slowest signal.

In contrast the PVDF signal with the fastest rising speed is the signal produced by the sensor that has not been shielded with tape, and therefore only has a thin layer of cyanoacrylate glue between the sensor and the metal cap.

Even with no tape shielding it was observed that the PVDF sensor does not appear to be as fast as the PCB® 113B21 SN 21794 sensor, to which it was compared, however this cannot be concluded for sure because it is the voltage that was compared rather that the pressure due to lack of calibration.

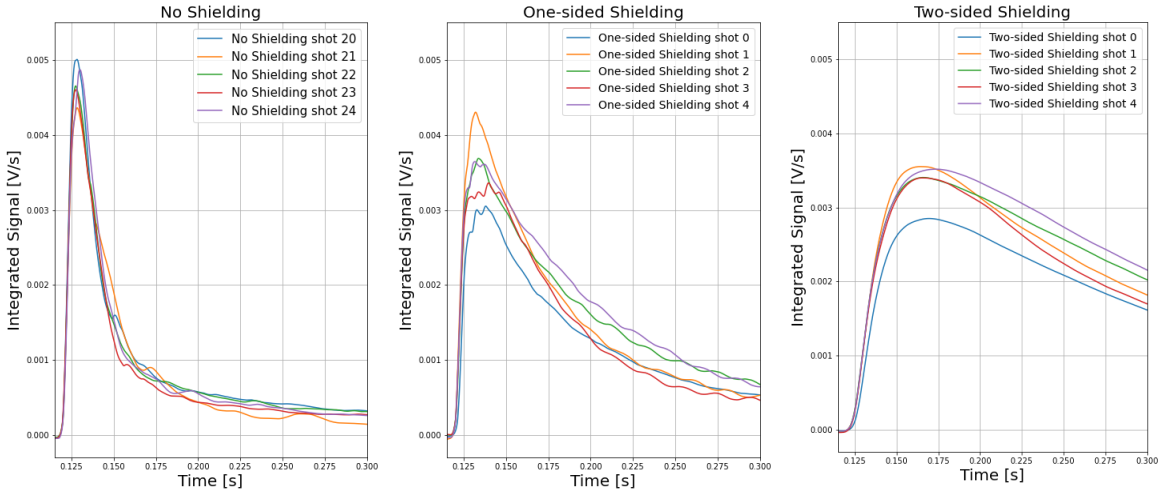

(a) (b) (c)

Figure 3.9. (a) Signals obtained with PVDF with no shielding; (b) Signals obtained with PVDF with one-sided shielding (c) Signals obtained with PVDF with two-sided shielding; All signals were obtained in voltage mode and integrated, data acquisition was assured by a portable data recorder (model: 1-GEN3i-2), tests conducted for a pressure of 8 bar.

In terms of signal reproducibility, the sensor with no shielding and the sensor with two-sided shielding provide quite good results, Figure 3.9 (a) and (c). Figure 3.9 (b) shows the signals obtained for PVDF with one-sided shielding, which are the least reproducible of the three.

3.3.3. Alternative Sensor Holder – Ceramic Backing

It was later suggested that perturbances might have been introduced in the signal due to metal bulging from the brass cap that composes the holder of the sensor. To study this possibility, a new holder was designed in which a layer of ceramic mainly composed of Alumina was added between the sensor and the metal cap. Figure 3.10 (a) and (b) show the described alterations made to the holder.

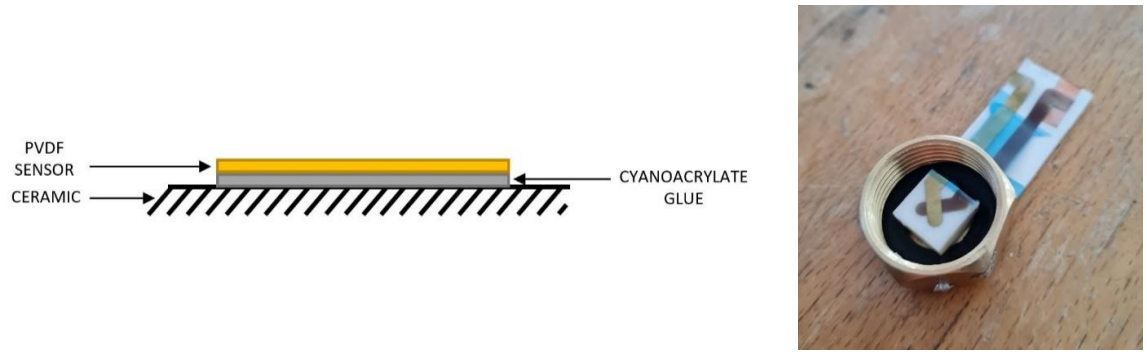

(a) (b)

Figure 3.10. (a) Illustrative example of PVDF sensor with no shielding and a ceramic backing; (b) Photograph of PVDF sensor with no shielding and a ceramic backing.

Seeing that the best results from the experiments with different shielding came from the sensor without it, it was decided that this sensor should too be applied with no shielding and bonded with as cyanoacrylate. This sensor was compared with the sensor without shielding as well as with PCB® no. 21794.

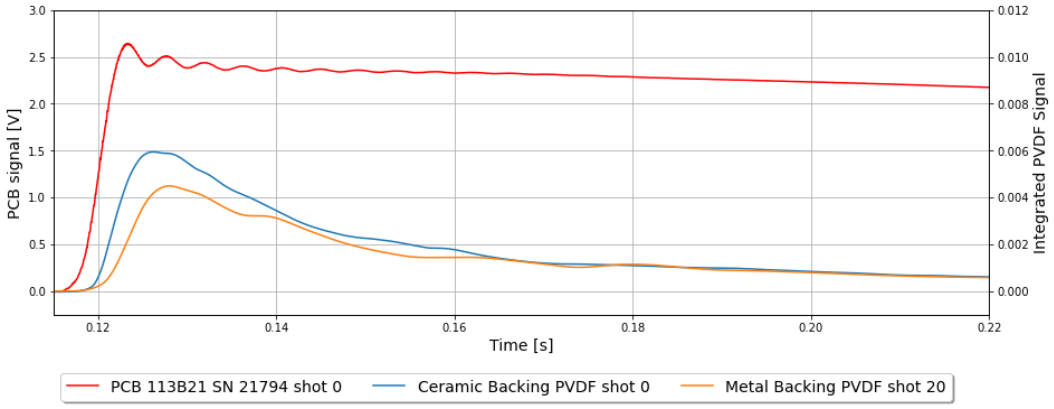

Figure 3.11. PVDF (with different backings) sensors and PCB® sensor signals for a pressure of approximately 8bar measured with a portable data recorder (model: 1-GEN3i-2).

The PVDF with a ceramic backing shows an even faster rising speed that the PVDF with metal backing, Figure 3.11, which, as already mentioned, is the PVDF with no shielding presented in the previous section. This makes the PVDF with a ceramic backing the one with the fastest rising speed. Having a ceramic backing also improved the reproducibility of the signal, Figure 3.12.

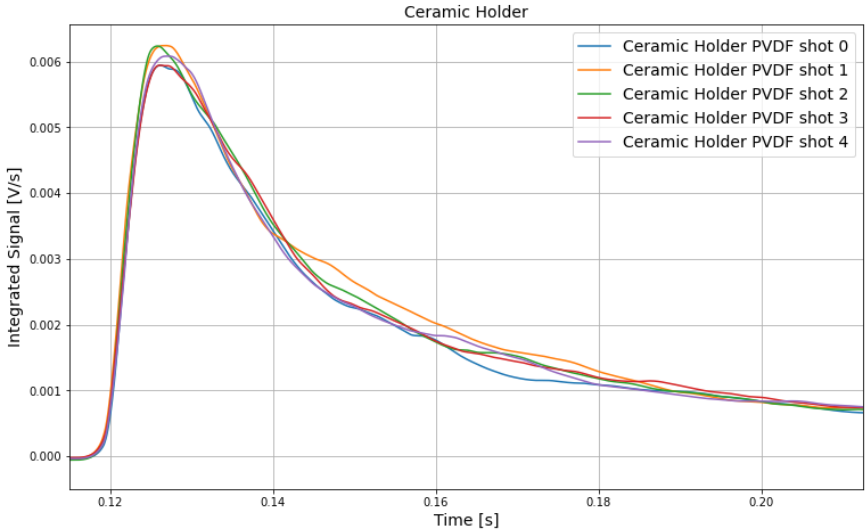

Figure 3.12. PVDF Sensor with ceramic backing signals for a pressure of approximately 8bar measured in voltage mode with a portable data recorder (model: 1-GEN3i-2).

3.3.4. Signal Difference for Distinct Measurement Modes.

Signal differences were observed between sensor signals at the same pressure, while measuring with different measurement modes. It was observed that charge mode measurements presented a longer and smoother shaped signal when compared to the signals obtained in voltage mode which presented a more irregular and noisier signal.

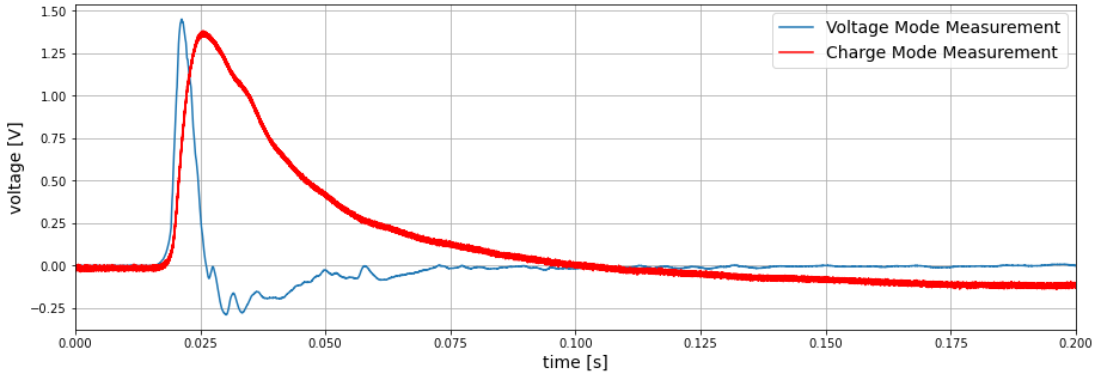

Figure 3.13. PVDF Sensor with ceramic backing signals for a pressure of approximately 8bar measured in voltage mode with a portable data recorder (model: 1-GEN3i-2).

The reason for this phenomenon is that in this experiment the condition RC $>>$ t, previously presented in section 2.1.3.1, was not validated and therefore the signal obtained in voltage mode did not represent the pressure versus time but instead returned a time derived

representation of the pressure. A solution for this was the integration in time of the voltage signal, Figure 3.14 (b).

After integration the voltage mode signal strongly resembles the charge mode signal, which corroborates the hypothesis that integration is required for the voltage signal measurement when complying with the condition $RC >> t$ is not possible. Figure 3.14 shows a comparison of the charge mode and integrated voltage mode measurement signals.

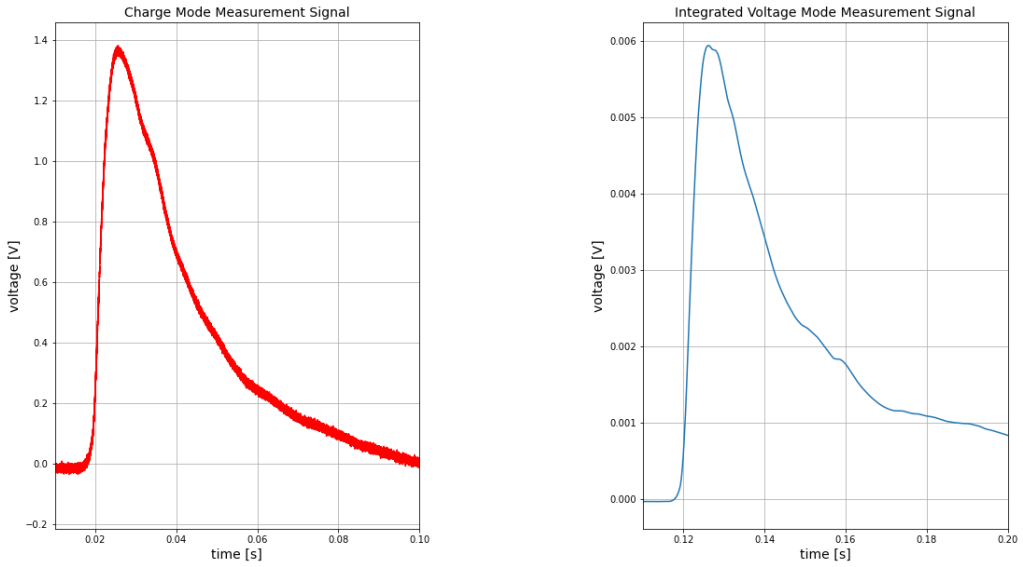

(a) (b)

Figure 3.14. (a)Example of a Charge mode measurement at approximately 8 bar; (b) Example of an Integrated Voltage mode measurement at approximately 8 bar.

Integration of the signal was accomplished using the "cumulative_trapezoid()" function from the SciPy library for python.

3.3.5. Sensor Calibration

For all the obtained results the acquisition chain's capacitance was measured and calibration of the PVDF sensors was attempted, using equations (2.4) and (2.5), however the obtained pressure value was off by a large factor.

Calibration was then carried out based on the pressure measured by the calibrated static pressure sensor. A calibration coefficient was obtained for each measured pressure in voltage

mode of each sensor by dividing the average target pressure by the maximum of the signal, i.e., the peak of the signal, of the average of all signals obtained for that specific pressure. These coefficients were denominated K_{PVDF_8bar}, K_{PVDF_6bar}, K_{PVDF_4bar} and K_{PVDF_2bar} for pressures of 8,6,4 and 2 bar respectively.

Since in charge mode, measurements were only made for 8 bar with each of the different sensor holder types, calibration can only be obtained for that specific pressure.

Table 3.1. All Calibration coefficients obtained for integrated voltage mode measurements.

Sensor	Two-sided shielding	One-sided shielding	No shielding	Ceramic Backing
K_{PVDF_8bar} [bar · s/V]	2426.29	2280.85	1812.20	1322.56
K_{PVDF_6bar} [bar · s/V]	2353.50	2301.59	1769.76	1363.10
K_{PVDF_4bar} [bar · s/V]	2244.74	2424.48	1869.93	1437.29
K_{PVDF_2bar} [bar · s/V]	2265.53	2557.83	2147.14	1572.34
K_{PVDF_8642} [bar · s/V]	**2322.51**	**2391.19**	**1898.51**	**1423.82**

The integrated value of the voltage signal should be multiplied by the coefficients presented in Table 3.1, so that the representation of the pressure versus time can be achieved, [bar] is the unit of pressure obtained by this operation.

The average measurement error associated with this calibration was also calculated using equation (3.1) where P_{PVDF} is the pressure measured by the PVDF sensor obtained using the global calibration coefficient, K_{PVDF_8642}, and P_{Target} is the target pressure measured by the static pressure sensor.

$$\text{Error } [\%] = \frac{P_{PVDF} - P_{Target}}{P_{Target}} \tag{3.1}$$

The measurement error associated with the global coefficient is presented in Table 3.2. Lower measurement errors are generally obtained for the pressures of 8, 6 and 4 bar. Higher measurement errors are mostly obtained for a pressure of 2 bar.

Table 3.2. Measurement error associated with K_{PVDF_8642}.

Sensor		**Two-sided shielding**	**One-sided shielding**	**No shielding**	**Ceramic Backing**
$\mathbf{K_{PVDF\_8642}}$ [bar · s/V]		2322.51	2391.19	1898.51	1423.82
Average measurement error	8 bar	-4.28 %	4.83 %	4.76 %	7.65 %
	6 bar	-1.32 %	3.89 %	7.27 %	4.45 %
	4 bar	3.46 %	-1.37 %	1.80 %	-0.94 %
	2 bar	2.51 %	-6.51 %	-11.58 %	-9.45 %

The calibration coefficients calculated for the charge mode measurements are presented in Table 3.3. Since charge mode measurements were only made for a pressure of approximately 8 bar only K_{PVDF_8bar} was obtained.

Table 3.3. Calibration coefficients obtained for charge mode measurements.

Sensor	**Two-sided shielding**	**One-sided shielding**	**No shielding**	**Ceramic Backing**
$\mathbf{K_{PVDF\_8bar}}$ [bar/V]	9.74	6.53	4.62	5.67

4. UNDER WATER PRESSURE MEASUREMENT OF SHOCK INDUCED CAVITATION

Having studied the impacts of employing different adhesives and different casings on the signal of PVDF sensors through the previous experiments, chapter 3, one solution was discovered which produced the most accurate results. This allowed the design of a new experiment that would focus on the study of PVDF's capability for pressure measurement of shock induced cavitation under water.

A PVDF sensor with no shielding, glued with a cyanoacrylate to a ceramic backing, was the one used for this experiment. For calibration of the PVDF sensors, a calibrated PCB® 113B21 sensor was used for reference purposes.

4.1. Experimental Setup

This study required the acquisition of the pressure measurement as well as visualization of the cavitation bubble's behaviour to allow for the identification of the pressure peaks in the signal and for future study of bubble dynamics. Additionally, the generation of a cavitation bubble was also required. The experimental setup, Figure 4.1, was designed considering these requirements.

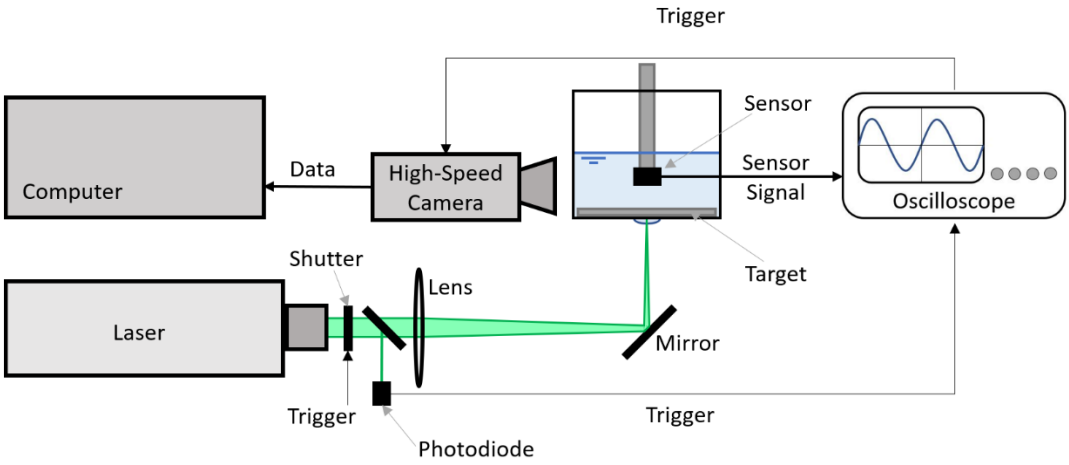

Figure 4.1. Experimental setup schematic.

A laser pulse with a 25 mm diameter beam is focussed trough a convergent lens with a focal length of 350 mm, reaching the target with a 5mm diameter. The target varied from

an 0.8 mm thick aluminium plate to a 4 mm and 6 mm thick ceramic plate composed of almost pure alumina. On the impact point, a water confinement, Figure 4.2 (a) and (b), was added to increase the shock wave pressure through the plate instead of dissipating into the air. This shock would then simultaneously generate shock wave and a cavitation bubble which upon collapse would create a secondary shock.

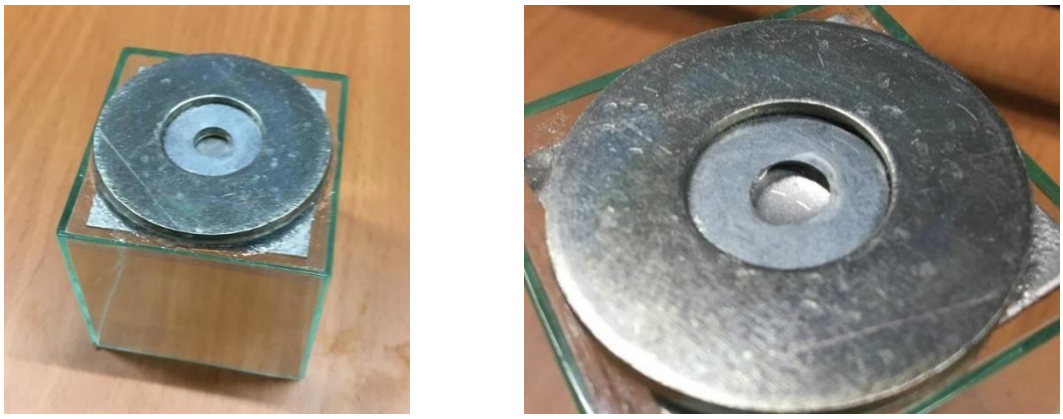

(a) (b)

Figure 4.2. (a)Upside down photograph of the 5 × 5 cm tank for show casing of the water confinement; (b) Zoom of the water confinement.

The pressure was measured with a PVDF sensor with a ceramic backing and with a PCB® 113B21 sensor (SN LW28294) for comparison purposes. Pressure signals were recorded on a RHODE&SCHWARZ® 10-bit RTM3004 oscilloscope with a time window of one millisecond.

Visualization of the cavitation bubble was assured by a high-speed camera recording at a frame rate of 200000 fps with a frame size of 256 × 128 pixels. A continuous light-emitting diode (LED) provided backlighting for the camera.

At $t = 0$s a trigger signal is sent to the laser shutter. A photodiode captures the light from the laser beam and sends a trigger signal to the oscilloscope. After receiving this signal, the oscilloscope sends a trigger signal so the high-speed camera so that all data acquisition devices start working at the same time.

The PVDF sensors are connected in voltage mode to the oscilloscope. For this experiment only voltage mode measurements were conducted. Since in this case $RC >> t$ is verified, the obtained signal is indeed a representation of the pressure versus time and not its derived representation.

Different targets were used in this study. Therefore, the experiments were divided in two parts: 4.1.1 - Experiments with an Aluminium Target and 4.1.2 - Experiments with a Ceramic Target.

4.1.1. Experiments with an Aluminium Target

As previously stated, in these experiments a laser pulse was shot at a 0.8 mm thick aluminium target. The selection of this target was due to its small thickness, which minimises shock absorption.

The medium where cavitation is generated and where the shock waves propagate until reaching the sensor, was also varied in other to evaluate the different possibilities of cavitation medium, that is, to evaluate if cavitation occurs in different mediums, and to evaluate the effect of shock wave absorption in these different mediums. Water, paraffin oil and paraffin gel, were the selected mediums for this study.

Due to the fact that the aluminium target was very thin and would bulge upon impact, the use of a PVDF sensor on top of the target was prevented and therefore the pressure is only measured at a distance, h = 9.64 mm of the impacted target. It is worth noting that this distance was obtained through image analysis which involves counting pixels turning it into a time-consuming method that is susceptible to error and uncertainty. The sensors used in this experiment were, as mentioned before, a PVDF sensor and a PCB sensor, for comparison and calibration purposes.

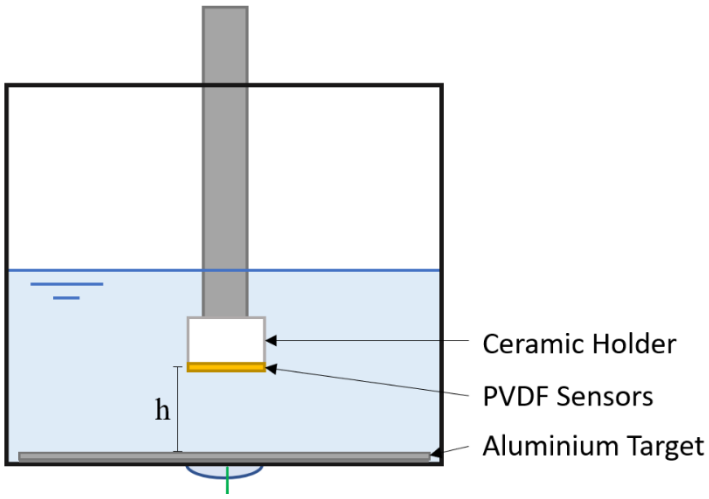

Figure 4.3. Experimental setup schematic of the 5 × 5 cm tank with an aluminium target.

4.1.2. Experiments with a Ceramic Target

A ceramic target was also used for experimentation. The laser shot was, however, not directly applied to the ceramic itself, instead a thin layer of aluminium tape was applied to the ceramic target so that the laser shock would be similar to the ones in the experiments with an aluminium target. The thickness of the tape as well as that of the adhesive layer are thin enough to be negligible.

This target allowed for the use of two PVDF sensors, one on top of the ceramic target and one at a distance a distance, h, from it, as shown in Figure 4.4. The distance h, obtained through image analysis, had a value of $h = 4.94$ mm for the 6 mm thick ceramic target and $h = 6.50$ mm for the 4 mm thick one.

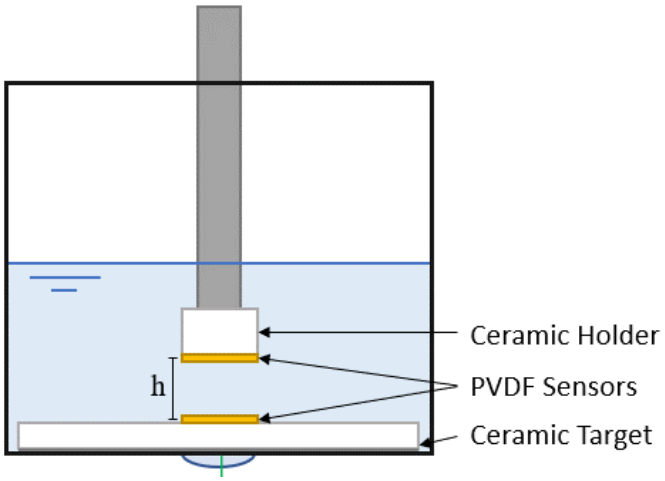

Figure 4.4. Experimental setup schematic of the 5 × 5 cm tank with a ceramic target.

For this experiment only PVDF sensors were used to measure the pressure created by the primary and secondary shocks created by the cavitation bubble's dynamics.

4.2. Experiment Results

The results form both experiments are presented in this section. Image analysis was used to verify the identity of the peaks measured by the sensor. The acquired signals were read and treated using Python through ANACONDA's *Jupyter Notebook*.

4.2.1. Aluminium Target Results

Experiments were conducted with different cavitation mediums to evaluate the difference in bubble dynamics as well as to evaluate the impact different mediums have on

the pressure measurements. As previously mentioned, three different mediums were considered in this experiment: water, paraffin oil and paraffin gel.

Different bubble sizes were observed when using different mediums, as shown in Figure 4.5. It can be observed that a bigger cavitation bubble is generated in the less viscous medium, water, Figure 4.5 (a), and smaller one is created in the most viscous one which is paraffin gel, Figure 4.5 (b). Additionally, while in water and in paraffin oil a single cavitation bubble is generated, this was not the case in paraffin gel. In the latter, multiple bubbles were generated at the same time and then merged into one larger bubble. After this merge the new cavitation bubble would slowly contract and eventually collapse like the ones created in the other two mediums.

It was also observed that the time variable was very different across the different mediums. From the growth of the bubble to its eventual collapse the bubble dynamics happened at a much faster pace for the mediums with a higher viscosity. Figure 4.5 shows that the growth peak of the bubbles in each medium happened at different times. In this case the bubble in paraffin gel reached its peak at 0.260 ms, the one in paraffin oil reached it at 0.380 ms and the one in water only stopped its growth at 0.415 ms.

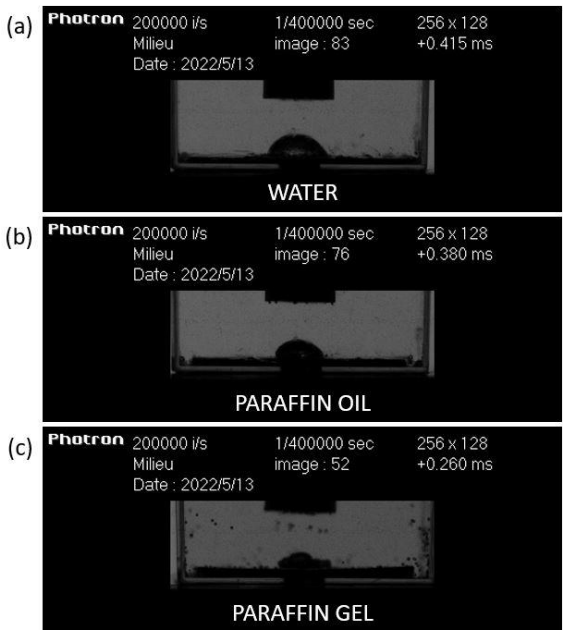

Figure 4.5. (a) Example of the growth peak of a cavitation bubble created in water; (b) Example of the growth peak of a cavitation bubble created in paraffin oil; (c) Example of the growth peak of a cavitation bubble created in paraffin gel; These bubbles were created by a laser pulse shot at an aluminium target.

Apart from the fact that in paraffin gel multiple bubbles were created upon impact and later merged and that the life of the bubble was much shorter in more viscous environments, the general bubble dynamics of this experiment were similar in each medium. Upon impact a cavitation bubble was generated, this bubble would then grow until reaching its peak after which it would rapidly decrease in volume and collapse. In some instances, mostly in water, a small cloud of micro bubbles or a ring-shaped micro jet was generated, their magnitude was, however, so small that almost no traces are found in the signal. Figure 4.6 presents a series of images that show an example of the bubble dynamics when in water. In Figure 4.6 (14) the collapse of the bubble is observed while in Figure 4.6 (15) and (16) a lingering cloud of micro bubbles can be observed.

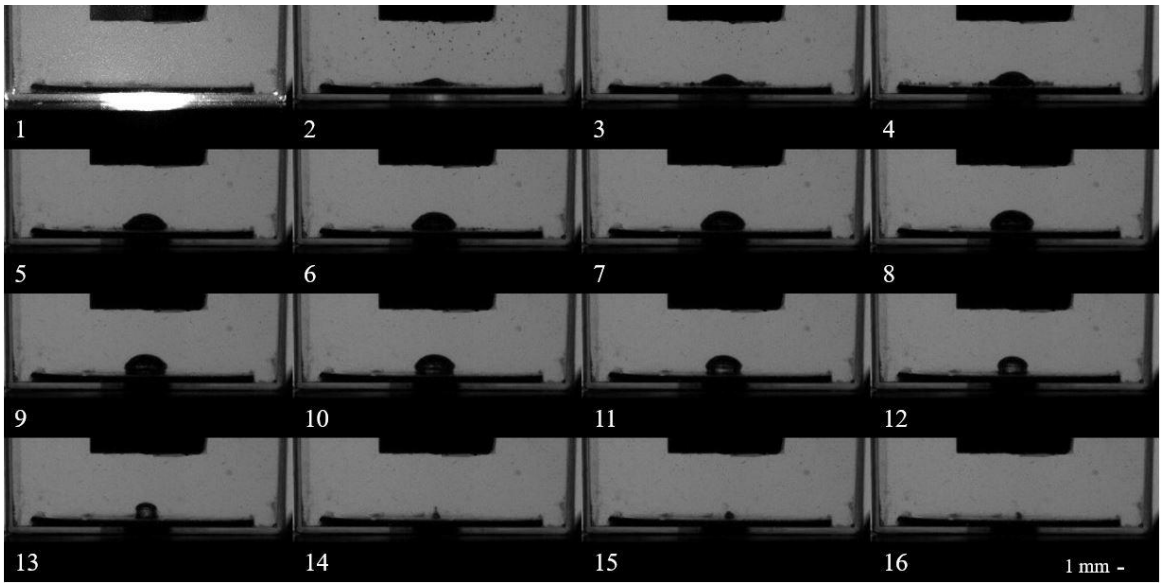

Figure 4.6. Behaviour example of a shock induced cavitation bubble in water with a ceramic target; the presented series of images are at a constant time step apart from each other.

PVDF sensor measurements corroborate the hypothesis that the cavitation bubble dynamics happen at a faster rate in more viscous environments. Figure 4.7 shows an example of the acquired signals with a PVDF sensor, where the time interval between both shocks represents the lifespan of the generated bubble.

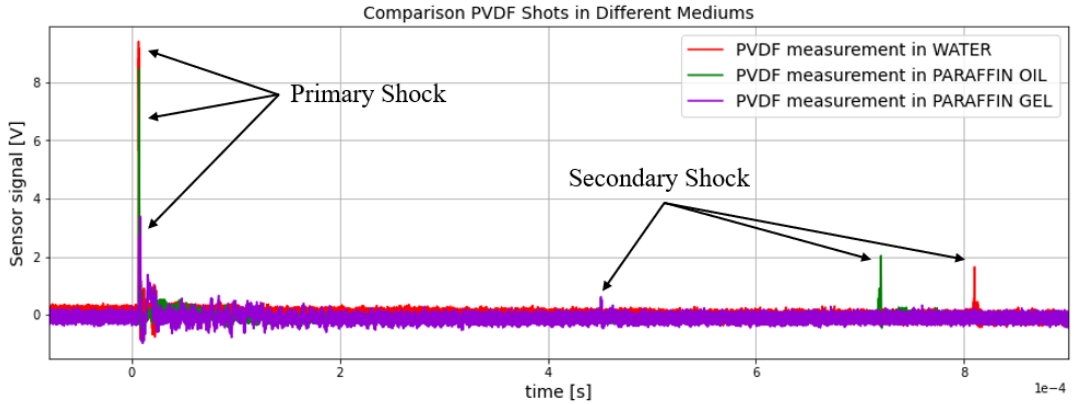

Figure 4.7. PVDF sensor measurements in different mediums.

The primary shock corresponds to the shock created by the laser pulse, which is the cause of the bubble, on the other hand, the secondary shock is caused by the collapse of the bubble. Additionally, the signals in Figure 4.7, also show that higher pressures are measured for water and liquid paraffin. Upon closer inspection of the acquired signals, Figure 4.8, it was observed that the signals acquired for paraffin gel behaved in an odd manner when compared to the remaining signals. This signal does not rise to the same magnitude as the signals obtained in other mediums, nor does it have a similar shape to them.

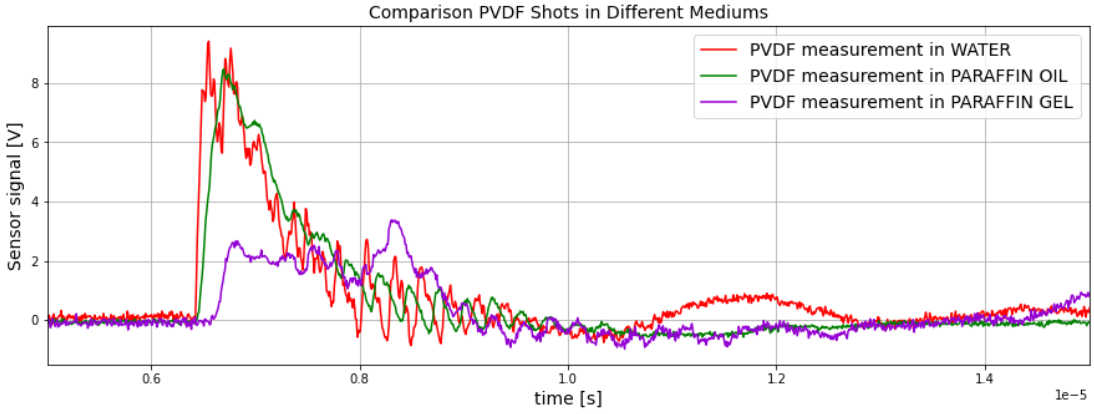

Figure 4.8. Zoom of the primary shock of PVDF sensor measurements in different mediums.

When compared to the PCB® 113B21 (SN LW28294) sensor the PVDF gauge appeared to present results with a higher rising speed when compared to the PCB® sensor. This is represented in Figure 4.9, once again this is not an accurate conclusion since the voltage is being compared and not the pressure.

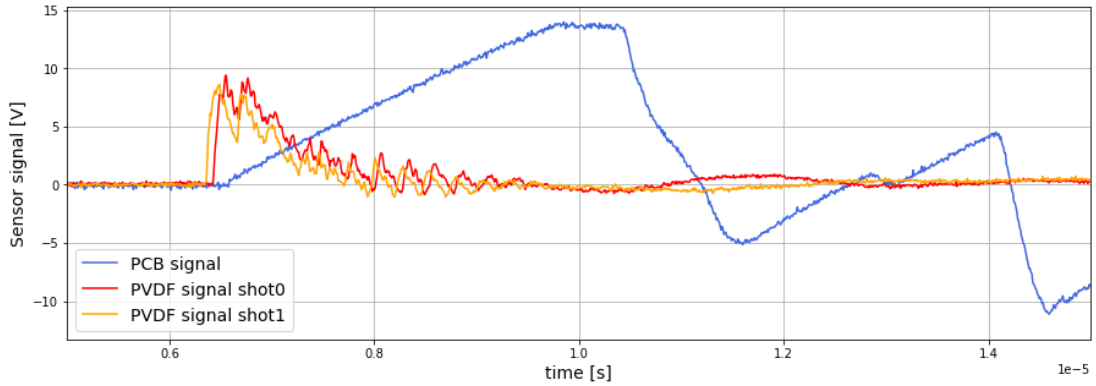

Figure 4.9. Comparison of PVDF and PCB® 113B21 sensor signals for the primary shock of the cavitation bubble generated in water.

Calibration of the PVDF sensors based on the pressure measured by PCB® 113B21 was not possible, due to the fact that overpressures of over 40 bar were reached which is over the limits of the measurement range of PCB® 113B21 sensors.

4.2.2. Ceramic Target Results

Preliminary tests were conducted to verify if cavitation would occur when the laser pulse was shot at a ceramic target and the response was positive. Ceramic targets of different thickness, 6 and 4 mm, were used for these preliminary tests, however since smaller bubbles were created with the 6 mm ceramic target, it was decided that for this study experiments should focus on 4 mm ceramic target.

Additionally, it was observed that only one shot could be made in each ceramic target since after one shot had been made, if a second one was attempted the measured primary shock pressure would be much lower than for the first shot, Figure 4.10 (a) and (b). It is thought that after one shot the ceramic target would break and lose its ability to properly transfer the shock created upon impact to the water.

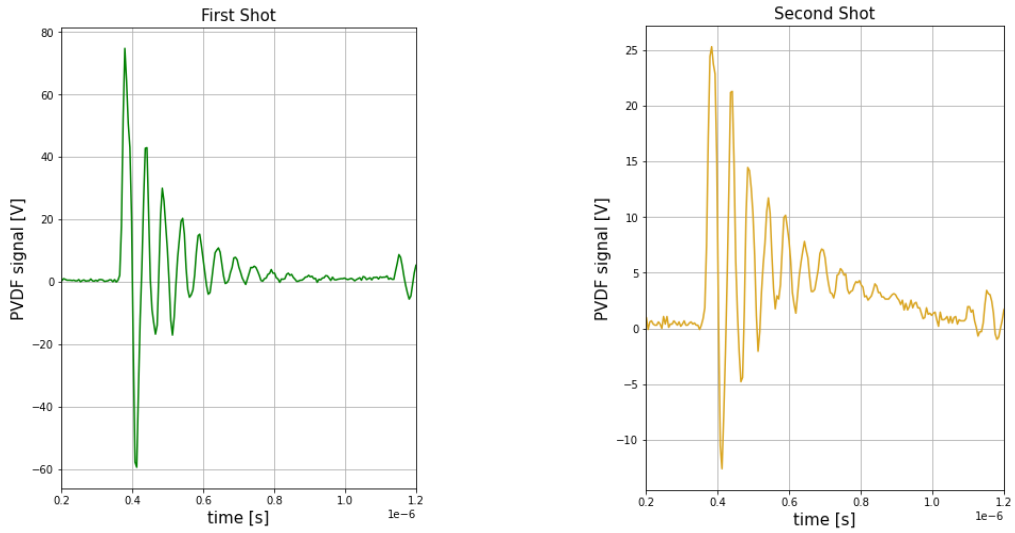

(a) (b)

Figure 4.10. (a) Primary shock of the first shot made in a specific ceramic target; (b) Primary shock of the second shot made in the same ceramic target

Two PVDF sensors were used in these experiments, as mentioned in section 4.1.2, one was placed on top of the ceramic target, and the other at a set distance, $h = 6.5$ mm, from the target.

The obtained results show that the pressure measured at the target, where the bubble is created, is much higher, around 10 times higher, than the pressure measured at a distance of 6.5 mm, Figure 4.11. This happens because when the energy is transferred from the target into the bubble, the bubble will disperse the energy in multiple directions instead of just one.

Additionally, it can be observed that the primary shock is measured by the PVDF sensor on the target around 4.3 μs sooner than on the other PVDF sensor. This time lapse can also be calculated through equation (4.1), where C_w is the speed of sound in water at room temperature, approximately 1500 m/s, h is the distance between the sensors and τ is the time it takes for the shock wave to travel the distance between sensors.

$$\tau = \frac{h}{C_w} \tag{4.1}$$

Through this equation the value of the timelapse between the signals is $\tau = 4.3333 \times 10^{-6}$ s which is close to the value obtained by analysing the graph in Figure 4.11.

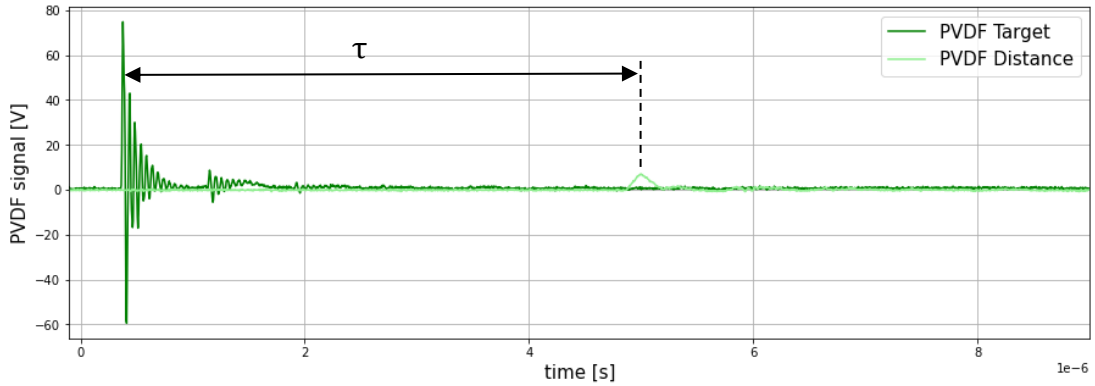

Figure 4.11. Comparison of PVDF signals, measured at the target and at a 6.5 mm, distance for the primary shock of the cavitation bubble generated in water.

The behaviour of the cavitation bubble when generated with the ceramic target is very similar to that of the bubble generated by an aluminium target, Figure 4.12. The bubble is generated upon impact, growing until it reaches its maximum radius after which it rapidly contracts and collapses. The main difference is that for a ceramic target the bubble is much smaller and its lifespan is considerably shorter.

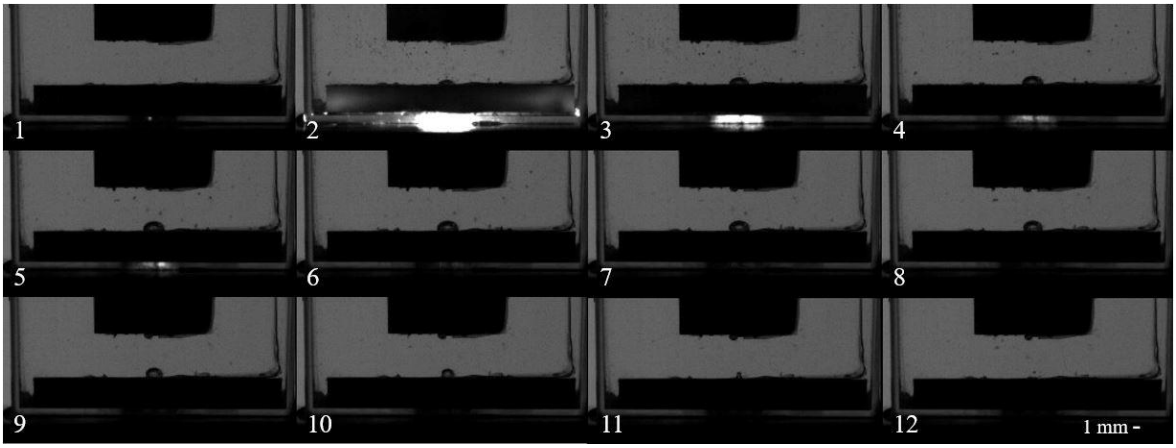

Figure 4.12. Behaviour example of a shock induced cavitation bubble in water with a ceramic target; the presented series of images are at a constant time step apart from each other.

5. CONCLUSIONS

A study for the calibration and better understanding of PVDF gauges was conducted, with the aim of introducing PVDF shock gauges in future larger scale experiments in the scope of the ProBalCav project.

Two different bonding agents were studied for use with PVDF, considering their impact on the signal as well as the practicality of their use. It was concluded that for prototyping purposes in which accuracy is not the main goal silicone grease is a good candidate, however if signal reproducibility and better accuracy are required the use of cyanoacrylates is recommended.

Several combinations of materials were considered for the casing of the sensor. It was found that having a ceramic backing greatly increased signal reproducibility and rising speed. It was also concluded that to vinyl tape is not a good candidate for mechanically shielding the active area of the sensor since it will greatly impact the acquired signal.

Interesting signals were captured by PVDF sensors when measuring the underwater pressure caused by the dynamics of a shock induced cavitation bubble. Calibration, however, was not possible due to the fact that pressures over 40 bar were reached which are over the limits of the measurement range of PCB® 113B21 sensors. Nevertheless, since there is a linear relationship between the applied pressure and the output voltage for the range of measured pressures, it was observed that a significant drop in the pressure is measured, approximately 10 times lower, at a distance of 6.5 mm from the target.

Further experimentation is required to fully understand the working of PVDF gauges so that calibration can be obtained without the need for a reference. It is proposed that calibration should be attempted in a setup where the condition $RC >> t$ is verified so that a calibration coefficient can be obtained prior to larger scale experiments. Using a shock tube for calibrating PVDF in voltage mode is one possible solution for this problem.

Additionally, since pressures higher that 40 bar are to be expected when dealing with cavitation phenomena, higher pressures should be reached on calibration of the sensor, as well as a sensor with a higher range of measurement than PCB® 113B21 sensors should be used for reference if needed.

BIBLIOGRAPHY

Arrigoni, M., F. Bauer, S. Kerampran, J. le Clanche, and M. Monloubou. 2018. "Development of a PVDF Pressure Gauge for Blast Loading Measurement." *Human Factors and Mechanical Engineering for Defense and Safety* 2 (1). https://doi.org/10.1007/s41314-018-0012-2.

Fourest, Thomas, Jean Marc Laurens, Eric Deletombe, Jacques Dupas, and Michel Arrigoni. 2014. "Analysis of Bubbles Dynamics Created by Hydrodynamic Ram in Confined Geometries Using the Rayleigh–Plesset Equation." *International Journal of Impact Engineering* 73 (November): 66–74. https://doi.org/10.1016/J.IJIMPENG.2014.05.008.

Grandjean, H., N. Jacques, and S. Zaleski. 2012. "Shock Propagation in Liquids Containing Bubbly Clusters: A Continuum Approach." *Journal of Fluid Mechanics* 701 (June): 304–32. https://doi.org/10.1017/jfm.2012.159.

Han, Zhaofeng, Cyril Mauger, Thibaut Chaise, Thomas Elguedj, Michel Arrigoni, Mahmoud el Hajem, and Nicolas Boisson. 2021. "Experimental and Analytical Study of under Water Pressure Wave Induced by the Implosion of a Bubble Generated by Focused Laser." https://doi.org/10.3390/s21144800.

"Products - Aifp-Bauer." 2022. May 31, 2022. https://aifp-bauer.fr/index.php/products/.

Ueberschlag, Pierre. 2001. "PVDF Piezoelectric Polymer." http://www.emerald-library.com/ft.

"WiSTL Gas Dynamics Calculator." 2008. 2008. http://silver.neep.wisc.edu/~shock/tools/gdcalc.html.

APPENDIX A

PCB® Sensor Calibration Table.

PCB TYPE	PCB NO.	8 bar test name	6 bar test name	4 bar test name	K_PCB_Average [V/bar]
113B21	SN 21794	3SR_AL01	3SR_AL02	3SR_AL03	0.3500
113B21	SN 21791	3SR_AL01	3SR_AL02	3SR_AL03	0.3150
113B21	SN 21793	3SE_AL04	3SR_AL05	3SR_AL06	0.3300
113B21	SN LW28294	3SE_AL04	3SR_AL05	3SR_AL06	0.3350
113B21	SN LW28295	3SE_AL07	3SR_AL08	3SR_AL09	0.3750
113B27	SN 42611	3SE_AL10	3SR_AL11	3SR_AL12	0.7250
113B27	SN 42613	3SE_AL10	3SR_AL11	3SR_AL12	0.6850
113B27	SN 42612	3SE_AL19	3SR_AL20	3SR_AL21	0.7150
113B28	SN LW35122	3SE_AL13	3SR_AL14	3SR_AL15	1.4650
113B28	SN LW35123	3SE_AL13	3SR_AL14	3SR_AL15	1.4350
113B28	SN LW35124	3SE_AL16	3SR_AL17	3SR_AL18	1.4450
113B28	SN LW35125	3SE_AL16	3SR_AL17	3SR_AL18	1.3950

The calibration coefficient was achieved by the average of the division of the maximum voltage of the PCB® sensor signal by the value of the target pressure, for three consecutive shots at the same pressure for each sensor.

APPENDIX B

In this appendix all the relevant shots made while conducting the cavitation experiments, as well as the resulting PVDF sensor and PCB sensor signals, are presented.

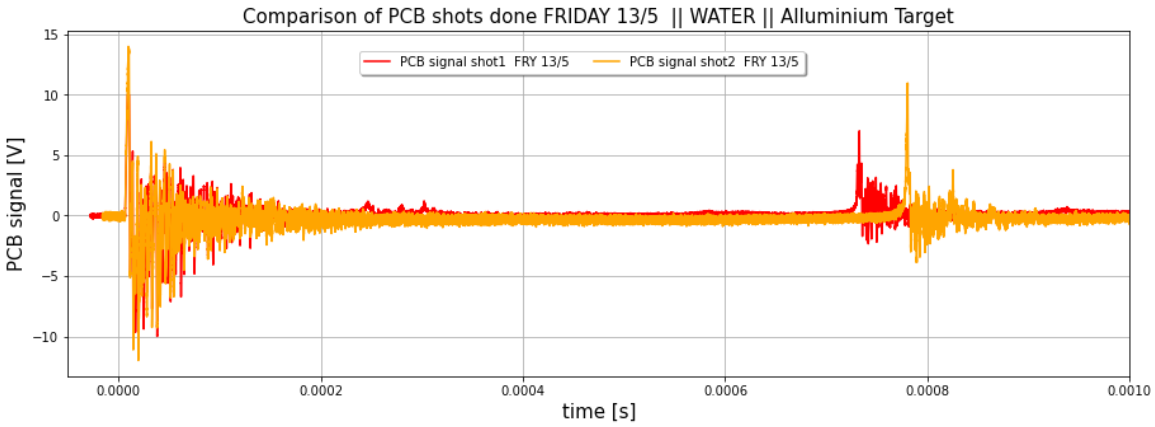

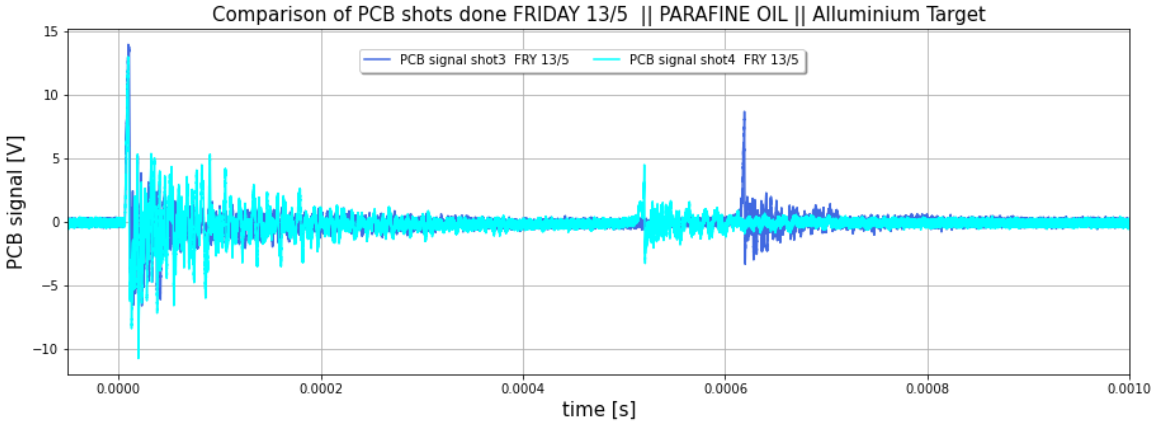

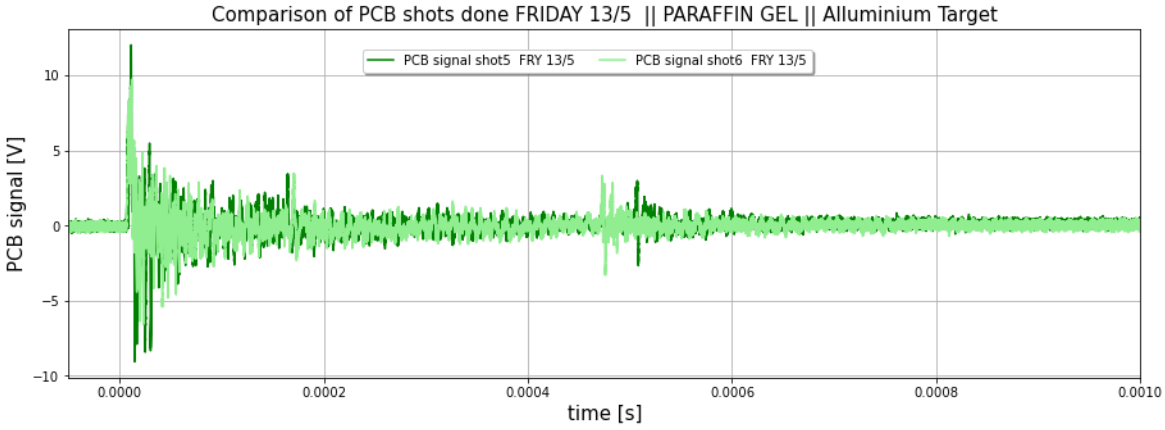

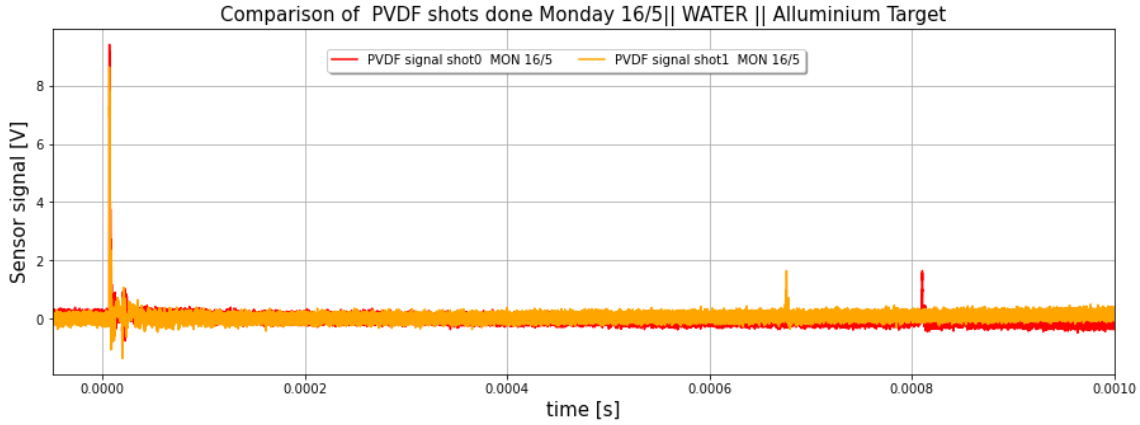
Comparison of PVDF shots done Monday 16/5|| WATER || Alluminium Target
PVDF signal shot0 MON 16/5
PVDF signal shot1 MON 16/5
Sensor signal [V]
time [s]

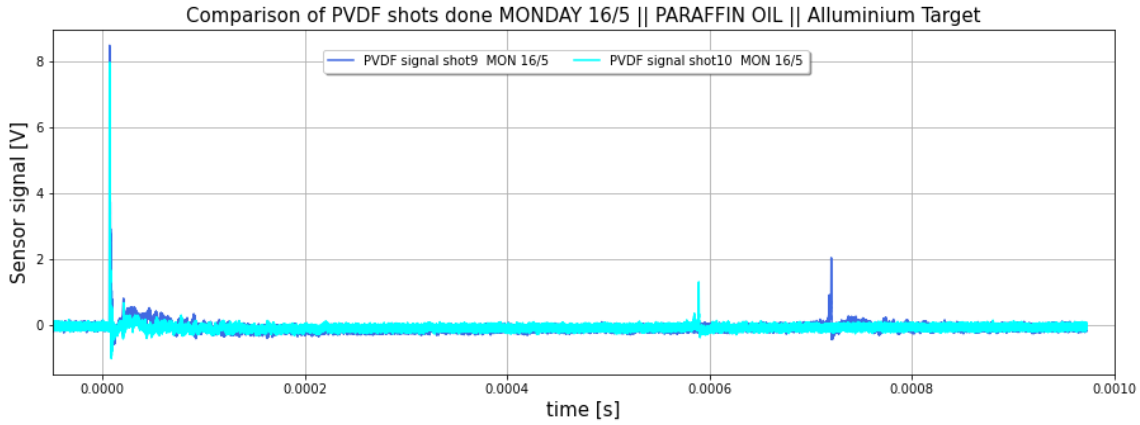
Comparison of PVDF shots done MONDAY 16/5 || PARAFFIN OIL || Alluminium Target
PVDF signal shot9 MON 16/5
PVDF signal shot10 MON 16/5
Sensor signal [V]
time [s]

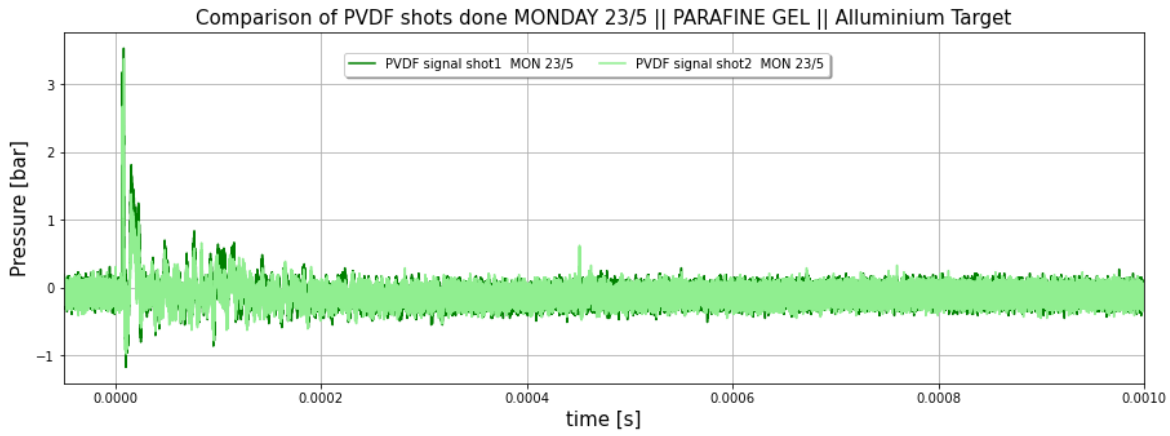
Comparison of PVDF shots done MONDAY 23/5 || PARAFINE GEL || Alluminium Target
PVDF signal shot1 MON 23/5
PVDF signal shot2 MON 23/5
Pressure [bar]
time [s]